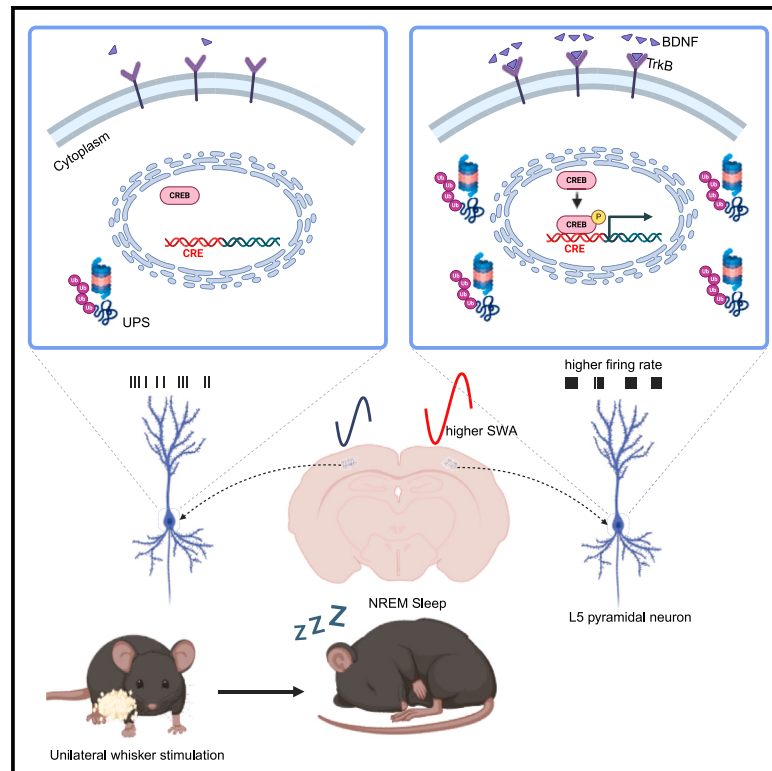# Cell Reports

BDNF-TrkB signaling orchestrates the buildup process of local sleep

Graphical abstract

Authors

Waleed ElGrawani, Guanhua Sun, Fabian P. Kliem, ..., Daniel B. Forger, Maria S. Robles, Steven A. Brown

Correspondence

wal33d91@gmail.com (W.E.),
antoine.adamantidis@dbmr.unibe.ch
(A.R.A.),
forger@umich.edu (D.B.F.),
charo.robles@med.uni-muenchen.de
(M.S.R.)

In brief

Local sleep is an intriguing observation across different species, but its regulation mechanism remains unclear. ElGrawani et al. report that BDNF-TrkB-CREB signaling plays a key role in the accumulation of local sleep pressure, a process that is mainly dictated by layer 5 excitatory pyramidal neurons.

Highlights

- Cortical BDNF controls local sleep SWA via TrkB activation in L5 pyramidal neurons

- BDNF/TrkB induction of local sleep SWA is CREB activity dependent

- TrkB activation induces ubiquitin and proteasome system activity

- Net synaptic weight potentiation in a mathematical cortical model upregulates SWA

CellPress

Article

BDNF-TrkB signaling orchestrates the buildup process of local sleep

Waleed ElGrawani,[1,2,13,*] Guanhua Sun,[3,10] Fabian P. Kliem,[4,10] Simon Sennhauser,[1] Sara Pierre-Ferrer,[1,2] Alex Rosi-Andersen,[1,2] Ida Boccalaro,[5] Philipp Bethge,[2,6] Won Do Heo,[7] Fritjof Helmchen,[2,6,8] Antoine R. Adamantidis,[5,11,*] Daniel B. Forger,[3,9,11,*] Maria S. Robles,[4,11,*] and Steven A. Brown[1,12]

[1]Institute of Pharmacology and Toxicology, University of Zurich, Zurich, Switzerland
[2]Neuroscience Center Zurich (ZNZ), University of Zurich, Zurich, Switzerland
[3]Department of Mathematics, University of Michigan, Ann Arbor, MI, USA
[4]Institute of Medical Psychology and Biomedical Center (BMC), Faculty of Medicine, LMU Munich, Germany
[5]Zentrum für Experimentelle Neurologie, Department of Neurology, Inselspital University Hospital Bern, Bern, Switzerland
[6]Brain Research Institute, University of Zurich, Zurich, Switzerland
[7]Department of Biological Science, Korea Advanced Institute of Science and Technology (KAIST), Daejeon 305-701, Republic of Korea
[8]University Research Priority Program (URPP), Adaptive Brain Circuits in Development and Learning, University of Zurich, Zurich, Switzerland
[9]Department of Computational Medicine and Bioinformatics, University of Michigan, Ann Arbor, MI, USA
[10]These authors contributed equally
[11]These authors contributed equally
[12]In memoriam
[13]Lead contact
*Correspondence: wal33d91@gmail.com (W.E.), antoine.adamantidis@dbmr.unibe.ch (A.R.A.), forger@umich.edu (D.B.F.), charo.robles@med.uni-muenchen.de (M.S.R.)
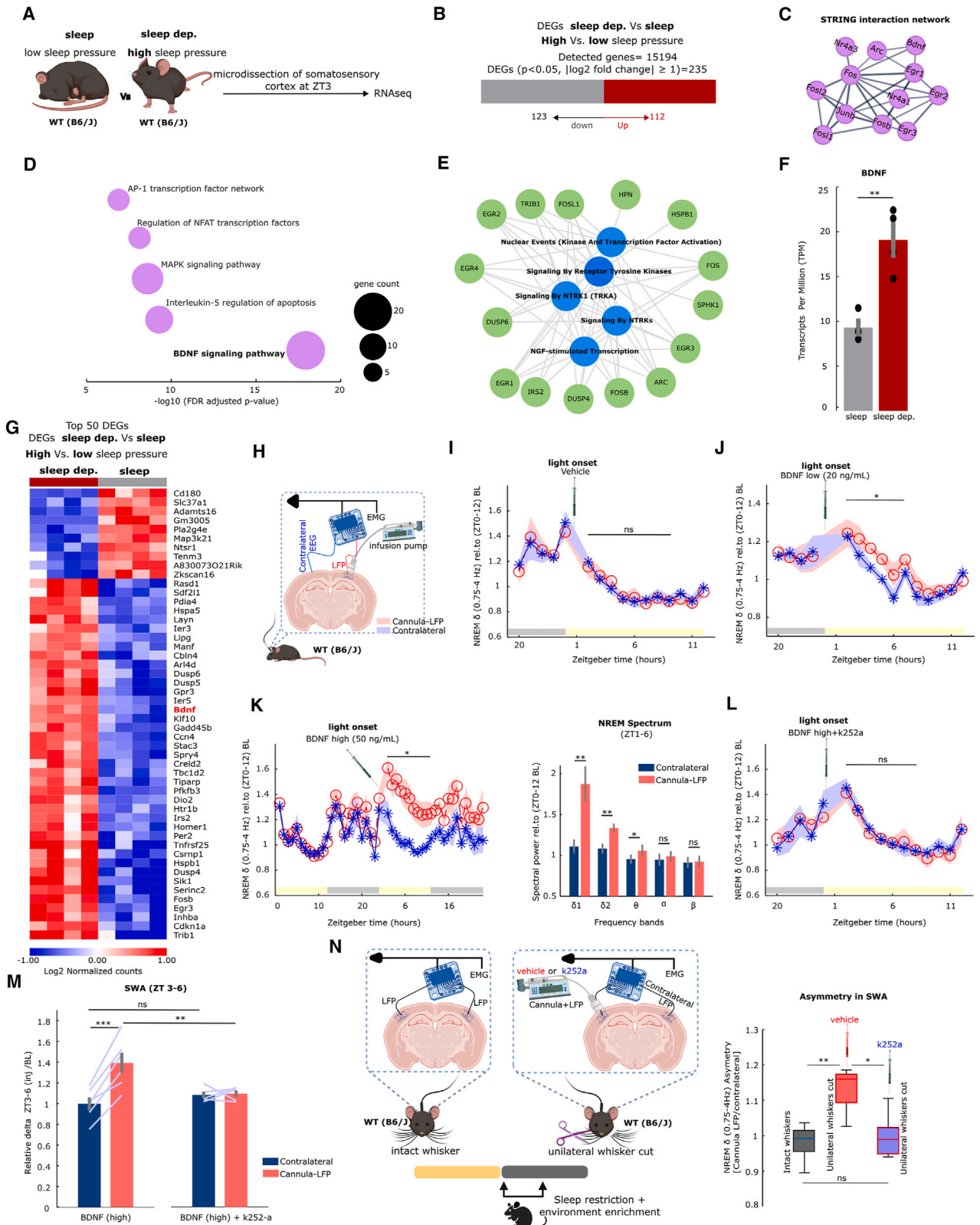https://doi.org/10.1016/j.celrep.2024.114500

SUMMARY

Sleep debt accumulates during wakefulness, leading to increased slow wave activity (SWA) during sleep, an encephalographic marker for sleep need. The use-dependent demands of prior wakefulness increase sleep SWA locally. However, the circuitry and molecular identity of this "local sleep" remain unclear. Using pharmacology and optogenetic perturbations together with transcriptomics, we find that cortical brain-derived neurotrophic factor (BDNF) regulates SWA via the activation of tyrosine kinase B (TrkB) receptor and cAMP-response element-binding protein (CREB). We map BDNF/TrkB-induced sleep SWA to layer 5 (L5) pyramidal neurons of the cortex, independent of neuronal firing per se. Using mathematical modeling, we here propose a model of how BDNF's effects on synaptic strength can increase SWA in ways not achieved through increased firing alone. Proteomic analysis further reveals that TrkB activation enriches ubiquitin and proteasome subunits. Together, our study reveals that local SWA control is mediated by BDNF-TrkB-CREB signaling in L5 excitatory cortical neurons.

INTRODUCTION

Sleep is a biological/physiological need that is tightly linked to brain processes occurring not only during sleep but also during wakefulness. In mammals, based on electroencephalogram (EEG) measurements, sleep consists primarily of two distinct stages: rapid eye movement (REM) and non-rapid eye movement (NREM). NREM sleep, which occupies approximately 80% of sleep time, is characterized by EEG slow and delta waves (SWs; ≤ 4 Hz).[1] The homeostatic need for sleep progressively increases with time awake until it reaches a threshold when sleep will be favored.[2] The spectral power of sleep SWs (SWA) noticeably increases after extended periods of wakefulness and dissipates across sleep episodes.[3] Therefore, SWA is widely considered as a hallmark of homeostatic sleep drive, reflecting prior wake duration and quality.[4,5]

Beyond its global manifestations, sleep SWs display notable gradual variations along the antero-posterior axis of the cortex[6] and exhibit a binary alternating SWs state between brain hemispheres in certain species, commonly referred to as "uni-hemispheric sleep."[7–9] This unique topographical distribution of sleep oscillations supports a local regulation of sleep or at least some of its features. Sleep SWs' amplitude varies temporally across cortical regions, reflecting task-dependent demands of prior wakefulness.[10–12] Indeed, sleep SWs can be locally regulated based on previous experience during wakefulness. This local increase in SWA during sleep has been suggested to foster local network functional integrity or restorative processes and is ultimately correlated with enhanced task performance after sleep.[11,13,14] This presumably implicates a molecular tracking of previous cellular activities during wakefulness for subsequent modulation of sleep SWs. Yet, the exact mechanisms and circuit underlying this process are far from being understood.

A sleep / sleep dep. — low sleep pressure / high sleep pressure — microdissection of somatosensory cortex at ZT3 → RNAseq — WT (B6/J) Vs WT (B6/J)

B DEGs **sleep dep.** Vs **sleep** / **High** Vs. **low** sleep pressure. Detected genes= 15194. DEGs (p<0.05, |log2 fold change| ≥ 1)=235. 123 ← down, Up → 112

C STRING interaction network

D AP-1 transcription factor network; Regulation of NFAT transcription factors; MAPK signaling pathway; Interleukin-5 regulation of apoptosis; BDNF signaling pathway. gene count 20 10 5. -log10 (FDR adjusted p-value)

E Nuclear Events (Kinase And Transcription Factor Activation); Signaling By Receptor Tyrosine Kinases; Signaling By NTRK1 (TRKA); Signaling By NTRKs; NGF-stimulated Transcription

F BDNF. Transcripts Per Million (TPM). sleep / sleep dep. **

G Top 50 DEGs. DEGs **sleep dep.** Vs **sleep** / **High** Vs. **low** sleep pressure. sleep dep. / sleep. Log2 Normalized counts -1.00 0.00 1.00

H EMG; Contralateral EEG; LFP; infusion pump; Cannula-LFP; Contralateral; WT (B6/J)

I light onset Vehicle. NREM δ (0.75-4 Hz) rel.to (ZT0-12) BL. ns. Zeitgeber time (hours)

J light onset BDNF low (20 ng/mL). NREM δ (0.75-4 Hz) rel.to (ZT0-12) BL. *. Zeitgeber time (hours)

K light onset BDNF high (50 ng/mL). NREM δ (0.75-4 Hz) rel.to (ZT0-12) BL. *. Zeitgeber time (hours). NREM Spectrum (ZT1-6). Spectral power rel.to (ZT0-12 BL). Contralateral / Cannula-LFP. δ1 ** δ2 ** θ * α ns β ns. Frequency bands

L light onset BDNF high+k252a. NREM δ (0.75-4 Hz) rel.to (ZT0-12) BL. ns. Zeitgeber time (hours)

M SWA (ZT 3-6). Relative delta ZT3-6 (inj /BL). ns *** **. BDNF (high) / BDNF (high) + k252-a. Contralateral / Cannula-LFP

N EMG; LFP; vehicle or k252a; Contralateral LFP; Cannula+LFP; WT (B6/J) intact whisker; WT (B6/J) unilateral whisker cut; Sleep restriction + environment enrichment. Asymmetry in SWA. NREM δ (0.75-4Hz) Asymmetry [Cannula LFP/contralateral]. vehicle / k252a. Intact whiskers / Unilateral whiskers cut / Unilateral whiskers cut. ** * ns

(legend on next page)

At the cellular level, cortical neurons exhibit various firing patterns in different states of vigilance.[15–17] Wakefulness is characterized by tonic firing patterns and typically higher firing rates compared to inactive periods.[18] In NREM, neurons show a distinct periodic shift between sustained firing ("ON") and quiescent periods ("OFF").[19–21] Upon extended wakefulness, cortical firing steadily further increases until it reaches a saturation level within the first 3 h of sleep deprivation, and in the subsequent recovery sleep, OFF periods are prolonged.[18] In vitro studies also demonstrated homeostatic regulation of cortical firing in cultured neurons, where stimulation with a cocktail of wake-promoting neuromodulators resulted in increased SWs' power (<1.75 Hz) during the washout phase.[22] Different tasks can be used to trigger local sleep homeostasis such as unilateral hand vibration or movement in humans[22] and unilateral whisker-cut to stimulate the usage of intact whiskers in rodents.[12,13] In both cases, the relevant cortical areas exhibited higher firing content relative to surrounding networks,[23–25] suggesting neuronal firing per se as a possible cause of cellular sleep pressure (i.e., fatigue) accumulated during wakefulness.

In addition, synaptic plasticity changes underlying learning during wakefulness may also account for sleep need.[26,27] Molecular substrates of synaptic plasticity, such as brain-derived neurotrophic factor (BDNF), are enriched during wakefulness.[28] Interestingly, BDNF levels not only increase as a function of wake duration but also reflect wake quality since exploratory behavior is associated with a proportional increase in BDNF and global SWA in subsequent sleep.[29] Bdnf gene transcription is tightly controlled by multiple promoters,[30] and its activity-dependent expression strongly relies upon activation of promoter IV.[31] Mice with a mutation in this promoter are unable to upregulate BDNF in an activity-dependent manner and exhibited reduced NREM SWA.[32] On the other hand, acute cortical microinfusion of BDNF significantly increased NREM SWA.[33] Yet, the intracellular mechanism and circuitry underlying BDNF effects on sleep SWA remain unexplored.

Here, we designed a local EEG assay[34] to investigate the molecular mechanisms underlying the accumulation of local sleep SWA. We used chemogenetics, optogenetics, and pharmacological approaches to explore intracellular mechanisms and to map cortical cells behind BDNF-dependent regulation of local sleep. We further characterized cortical transcriptome and proteome signatures driven by increased global or local SWA. Finally, we used mathematical modeling of a cortical network to better understand the impact of synaptic plasticity on SWA.

RESULTS

Cortical BDNF levels regulate local sleep SWA via activation of TrkB receptor

We explored the cellular mechanisms causing high cortical SWA levels using RNA-seq technology. To elevate cortical SWA levels, we sleep deprived (SD) a group of mice for 3 h starting at light onset (ZT 0), a well-documented approach to upregulate cortical SWA (Figure S1),[35] before they were sacrificed. Control mice were not SD and sacrificed at the same zeitgeber time (ZT 3). RNA-seq analysis of the somatosensory cortex from mice of both experimental conditions led to the quantification of 15,194 transcripts that met detection thresholds in both conditions (see STAR Methods). Of those, 235 transcripts were significantly differentially expressed ($p < 0.05$, |log2 fold change| $\geq$ 1) between conditions, with 112 being upregulated and 123 downregulated upon being SD (Figures 1A and 1B).

An interaction network analysis (using STRING, see STAR Methods) of the upregulated transcripts in SD ones revealed three significant clusters ($\geq$5 nodes/transcripts per cluster), with a top cluster (shown in Figure 1C) containing Bdnf and its regulated genes such as Fos and Arc. Concomitantly, gene set enrichment analysis (GESA) revealed that the Bdnf signaling pathway was the most significantly (Fisher's exact test, FDR-adjusted $p < 0.05$) enriched pathway with 21 annotated transcripts (Figure 1D). Reactome pathway analysis[36] also revealed a significant (Fisher's exact test, FDR-adjusted $p < 0.05$) enrichment of signaling by neurotrophin receptor kinases (NTRKs) as visualized in the reactome subnetworks in Figure 1E. Indeed, Bdnf transcript levels significantly increased after sleep deprivation, ranking among the top 50 most significantly differentially expressed transcripts (Figures 1F and 1G; see expression of Bdnf isoforms in Table S1). This is in line with previous studies showing elevated BDNF levels under similar conditions.[28,37–43] We also observed upregulation of transcripts that have been previously reported to increase upon SD in different contexts such

---

Figure 1. Cortical BDNF levels regulate local sleep SWA via activation of TrkB receptor

(A) Schematic of the experimental procedure for the study of transcriptome signatures between sleep and sleep deprivation.

(B) Horizontal bar plot showing the number of differentially expressed transcripts (DEGs; $n = 4$ mice per group).

(C) STRING interaction network for significantly upregulated transcripts.

(D) Bubble plot of enriched terms for upregulated transcripts (x axis, negative log10 [FDR-adjusted p value]; bubble size, count of significant genes in cluster).

(E) Reactome subnetworks for upregulated genes and enriched signaling pathways (top 5 pathways "reactome_2022"). Genes are in green and enriched pathways in blue.

(F) BDNF transcript abundance in sleep vs. sleep deprivation ($n = 4$, unpaired Student's t test, d = 3.6).

(G) Heatmap for the log2 normalized counts of the top 50 DEGs (unpaired Student's t test FDR-adjusted $p < 0.05$, |log2 fold change| $\geq$1). (H) Schematic for the experimental strategy.

(I–L) SWA time course upon the infusion of vehicle (I; $n = 4$, two-way RM ANOVA $p = 0.8397$), low-dose BDNF (J; $n = 4$, two-way RM ANOVA), high-dose BDNF (K [left]; $n = 6$, mixed-effects model "REML"), or BDNF + k252-a (L; $n = 5$, two-way RM ANOVA $p = 0.9780$). (K) (right) Power spectrum during NREM for the 6 h following high-dose BDNF infusion (paired Student's t test, $\delta1$: d = 2.1, $\delta2$: d = 2.1, θ: d = 1.5; Wilcoxon signed-rank, α: d = 0.5, β: d = 0.1).

(M) SWA (ZT 3–6) after infusion of BDNF alone or BDNF + k252-a, relative to baseline day (ZT 0–3). Local infusion of BDNF shows SWA upregulation compared either to contralateral or to BDNF + k252a infusion (respectively; paired Student's t test, d = 2.9; unpaired Student's t test, d = 2; after one-way ANOVA $p = 0.0022$).

(N) Schematic (left) of the experimental strategy. Boxplot (right) showing quantification of SWA as a ratio of cannula LFP/contralateral hemisphere at ZT 20 (unpaired Student's t test; after one-way ANOVA $p = 0.00883$; vehicle vs. intact, d = 2.4; k252a vs. vehicle, d = −2; $n = 5$ mice for intact, 4 mice for vehicle, and 5 mice for k252a). See also Figures S1 and S2.
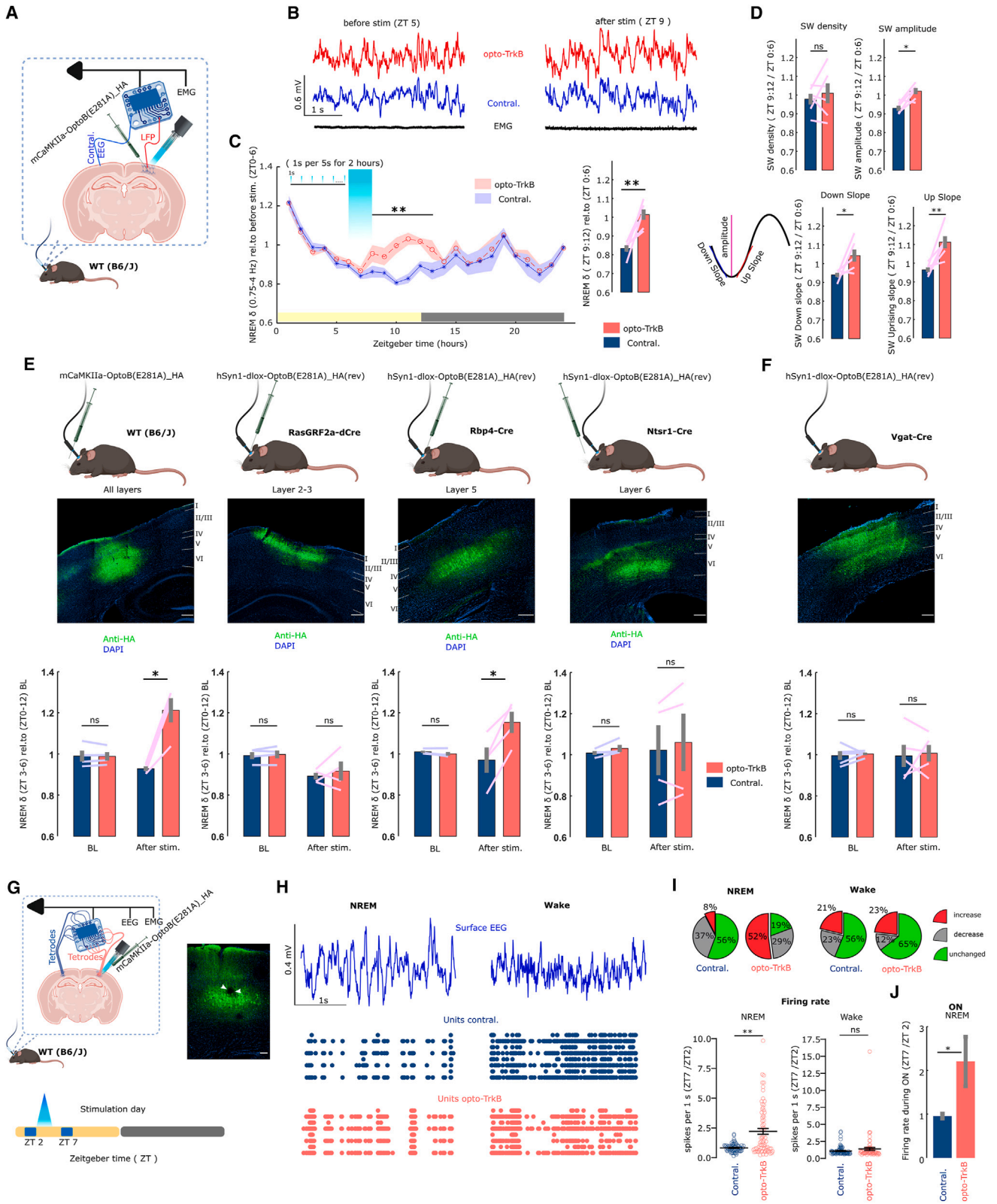
(legend on next page)

as *Homer1a*, *Fosb*, *Egr3*, and *Per2* (Figure 1G).[44–47] To summarize, our data show that the levels of *Bdnf* and its regulated genes/transcripts increased in the mouse somatosensory cortex in response to increased sleep debt, suggesting a possible role of BDNF-dependent signaling in local regulation of cortical SWA levels.

Indeed, a causal role of BDNF signaling in the regulation of sleep SWA in rats has been previously demonstrated by Faraguna and colleagues, showing a significant upregulation in sleep SWA upon the infusion of BDNF.[33] To further confirm the impact of BDNF on local SWA regulation in mice, we unilaterally infused BDNF, via an implanted cannula, and simultaneously recorded local field potential (LFP) signals from both the injection site and the contralateral hemisphere in freely moving mice (Figure 1H, see STAR Methods). We found that BDNF induced a dose-dependent upregulation of local SWA (0.75–4 Hz). The low dose of BDNF caused a delayed ($\approx$2–3 h after injection) increase in SWA that lasted for 3 h (Cohen's d = 0.9, Figure 1J), while the high dose resulted in a sustained SWA increase with a larger effect size (Figure 1K, Cohen's d = 3.4). The BDNF effect was specific to slow frequencies in delta and theta range, with bigger effect size in delta band as shown by spectrum analysis (Figure 1K). In addition, BDNF effects were only local and not due to adverse effects on the contralateral hemisphere (Figure 1M). As expected, control experiments in which only the vehicle was infused did not result in any local interhemispheric difference in SWA (Figure 1I). Thus, BDNF cortical levels play a key role in regulation of local cortical SWA levels.

BDNF is known to bind to tyrosine kinase B (TrkB) receptor with high affinity and to p75 neurotrophin receptor (p75NTR) with lower affinity.[48] To investigate whether TrkB receptor mediates the observed effects of BDNF on local sleep SWA, we co-infused BDNF with the blocker of TrkB receptor activation, k252-a (50 μM).[33,49,50] Consistent with the previous work of Faraguna and colleagues,[33] we found that TrkB activation inhibition

completely abolished the effects of BDNF on SWA, indicating that BDNF-dependent cortical SWA regulation is mostly mediated via TrkB receptor activity and its downstream signaling cascades (Figures 1L and 1M). In addition, we have unilaterally infused k252a (50 μM) alone and observed a slight but significant decrease in SWA in the 2 h following the infusion (Figure S2).

To further investigate whether the local experience-dependent upregulation of SWA is dependent on TrkB signaling, we unilaterally implanted mice with a cannula and performed a unilateral whisker trimming while ipsilaterally infusing either a vehicle or the TrkB inhibitor (k252-a) into barrel cortex (see STAR Methods). Mice whiskers were trimmed specifically at the beginning of the dark phase (ZT 12). Then, mice were kept awake for 4 h in an enriched environment to maximize explorative activities using their intact whiskers. As expected, mice that were unilaterally whisker trimmed and ipsilaterally injected with vehicle showed uni-hemispheric increase in subsequent NREM sleep SWA (Figure 1N). Interestingly, blocking TrkB activation eliminated the effect of unilateral whiskering on SWA asymmetry, suggesting that the local whisker-dependent SWA upregulation is mediated via the TrkB receptor activity.

BDNF-dependent regulation of local sleep SWA is largely mediated by L5 excitatory pyramidal neurons

To selectively investigate the implication of TrkB receptor in the upregulation of cortical SWA, we utilized an opto-activatable TrkB receptor (opto-TrkB).[51] We unilaterally injected *mCaM-KIIa-opto-TrkB-HA* adeno-associated virus 5 (AAV5) into the somatosensory cortex of wild-type (WT) mice to express opto-TrkB receptor in cortical pyramidal neurons and implanted an optical fiber for light delivery, while simultaneously recording LFP signals from the injection site and contralateral hemisphere (Figure 2A, see STAR Methods). We observed that optical activation of opto-TrkB-expressing cells with blue light (480 nm, 1 s per 5 s for 2 h) at either middle of light phase (ZT 6–8; Figure 2B and 2C)

Figure 2. BDNF-dependent regulation of local sleep SWA is largely mediated by L5 excitatory pyramidal neurons

(A) Schematic for the experimental strategy.

(B) Representative LFP (opto-TrkB), EEG (contralateral), and EMG traces during NREM before (left) and after (right) opto-TrkB stimulation.

(C) Time course (left) of SWA changes in response to opto-TrkB stimulation at ZT 6–8 (1-h bins; "REML"). Quantification (right) of SWA after stimulation (ZT 9–12) relative to before stimulation (n = 6, paired Student's t test, d = 2).

(D) Schematic (bottom left) of an SW. Bar plots showing analysis of various NREM SWs' morphology parameters including density (top left), amplitude (top right, d = 1.6), downward slope (bottom left, d = 1), and upward slope (bottom right, d = 1.8) for the same experiment in (C) (paired Student's t test).

(E) Schematic (top row) of the experimental strategy. Representative microscopic images (middle row) of opto-TrkB expression. SWA (bottom row) at ZT 3–6 in baseline and after optical stimulation that occurred at light onset (ZT 0–2) in 4 different mouse strains: (from left to right) WT B6/J (n = 4, d = 2.8), RasGRF2a-dCre (n = 4), Rbp4-Cre (n = 4, d = 2.9), and Ntsr1-Cre (n = 4) (paired Student's t test, scale bars: 200 μm).

(F) Identical to (E) for Vgat-Cre mice (right; n = 5, paired Student's t test).

(G) Schematic (top left) of the experimental strategy. Microscopic image (top right) confirming opto-TrkB expression and tetrode positioning in L5 (white arrow, scale bars: 100 μm). Experimental timeline (bottom): ZT 2 represents before stimulation recording, and ZT 7 represents after stimulation that occurred between ZT 2 and ZT 4.

(H) Representative surface EEG traces (blue, top row; filtered EEG between 0.625 and 100 Hz) and raster dot plots of units detected in opto-TrkB (light red, bottom rows) and contralateral (light blue, middle rows) cortical regions in NREM (left) and wake (right) states after optical stimulation. All units detected from one tetrode per site were represented (n = 1 mouse, 8 units from contralateral, 8 units from opto-TrkB, each spike is represented by a dot).

(I) Pie plots (top row) showing the percentage of units that increased (red), decreased (gray), or had unchanged (green) firing rate during NREM (2 pie charts on the left) and wake (2 pie charts on the right). The firing rate for each unit was considered to be changed if the unit has $\geq \pm$30% change in firing rate (i.e., firing rate in ZT 7/ZT 2 $\times$ 100 $\geq \pm$30%). Note the increase in percentage of units that upregulated firing rate in NREM sleep after opto-TrkB stimulation in comparison to contralateral hemisphere. Plots (bottom row) for the relative change in firing rate after stimulation during NREM (left; n = 73 units for opto-TrkB, n = 79 units of contralateral, d = 1) and wake (right; n = 75 units for opto-TrkB, n = 80 units for contralateral; n = 6 mice; Wilcoxon rank-sum test). Each unit is represented by a circle, and black lines represent mean $\pm$ SEM.

(J) Quantification of ON periods' firing rate during NREM (n = 6 mice, n = 10 tetrodes for opto-TrkB and 11 tetrodes for contralateral, Wilcoxon rank-sum test, d = 1). See also Figures S3–S7.

or light onset (ZT 0–2; Figure 2E) elevated local SWA levels with a delayed onset of ≈3 h. Power spectrum analysis revealed an increase in both δ1 and δ2 frequency bands in response to local opto-TrkB activation (Figures S4A and S5A). Since EEG SWA is a measure of SWs' density (i.e., frequency) or amplitude, we examined whether the opto-TrkB-dependent increase in SWA was a result of changes in wave amplitude, density, or both. Morphology analysis on NREM slow waves (0.75–4 Hz) indicated that the observed increase in SWA was due to an increase in amplitude and not due to change in SWs' densities (Figure 2D). Apart from amplitude, LFP SWs' slope has been suggested to reflect synchrony of cortical networks during transitions between active and silent states.[18,52] In our experiment, we observed steeper ascending and descending slopes in response to opto-TrkB activation, reflecting a higher degree of local network synchrony at transitions between SWs' "down" and "up" states (Figure 2D).

To further map cortical cells underlying regional SWA regulation, we stereotactically injected the Cre-dependent *hSyn1-dlox-optoTrkB-HA* AAV5 into the somatosensory cortex of three different transgenic mouse lines (*RasGRF2a-Cre, Rbp4-Cre, and Ntsr1-Cre*) to target the expression of opto-TrkB selectively to layers 2/3, 5, or 6, respectively.[53] This strategy effectively enriched opto-TrkB in the targeted cortical layers (Figure 2E). Optical activation of opto-TrkB in layers 5 (ZT 0–2) resulted in a significant increase in SWA (between ZT 3–6), similar to the results observed with opto-TrkB activation in all cortical layers (Figure 2E), whereas no significant interhemispheric changes in SWA were observed upon opto-TrkB activation in L2/3 or L6 (Figure 2E). Remarkably, repeated opto-TrkB stimulation (i.e., on the following day) in both WT and L5 significantly amplified local SWA levels, as depicted in Figures S3 and S4. It's worth mentioning that attempts to express opto-TrkB in L4 or L6 using *Nr5a1-Cre*[53] or *Syt10-Cre*[54] transgenic mice resulted in diverse expression across different cortical layers, without selective enrichment in the expected layers. As a result, these experiments were excluded from the analysis.

To further investigate the impact of activation of opto-TrkB exclusively on inhibitory interneurons, we unilaterally injected the Cre-dependent *hSyn1-dlox-optoTrkB-HA* AAV5 into somatosensory cortex of *Vgat-Cre* mice (see STAR Methods), a transgenic mouse line expressing Cre recombinase under the vesicular GABA (γ-Aminobutyric acid) transporter promoter.[55] In contrast to our previous results, we found that optical activation of opto-TrkB-expressing inhibitory cells at light onset (ZT 0–2) did not result in sustained increase in local SWA (Figure 2F). Taken together, these findings indicate that BDNF mediates upregulation of local SWA levels through the activation of TrkB in excitatory pyramidal neurons of layer 5 of the somatosensory cortex.
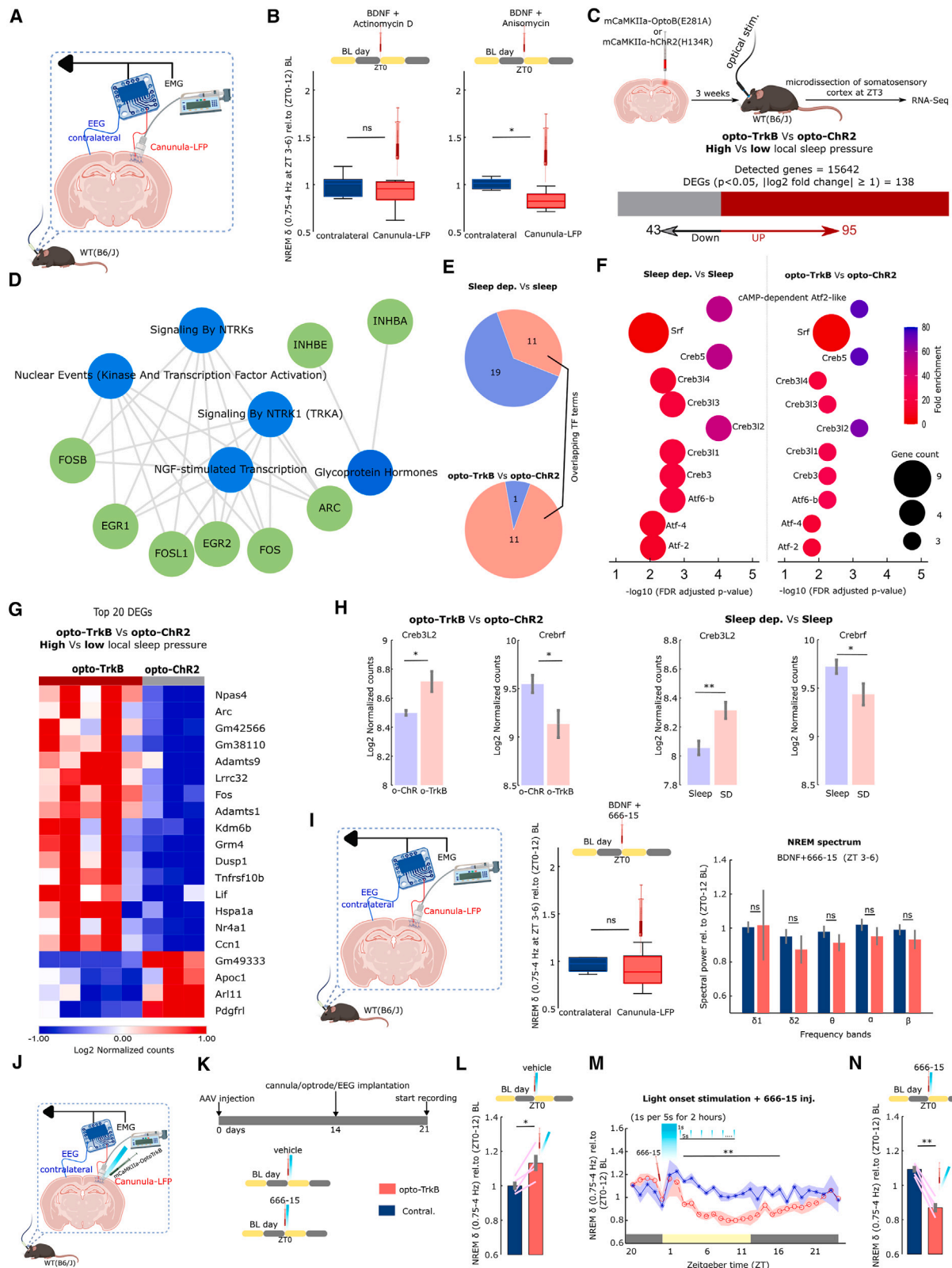
To gain insights into the effects of BDNF at single-cell resolution, we examined firing rates in response to local opto-TrkB receptor activation. We unilaterally injected *mCaMKIIa-opto-TrkB-HA* AAV5 and implanted an optical fiber, along with two tetrodes targeting L5 of the somatosensory cortex, while positioning two tetrodes on the contralateral hemisphere (Figure 2G, see STAR Methods). Successful opto-TrkB expression and accurate positioning of tetrodes was confirmed at the end of experiment (Figure 2G). In order to assess the effects of stimulation, we conducted recordings during two distinct hours of the day, specifically at ZT 1-2 and ZT 6-7, for both a baseline day and a stimulation day. During the baseline day, the mice were not subjected to any interventions, while on the stimulation day, they were optically stimulated (1 s every 5 s) for a period of 2 h (ZT 2–4). We selected ZT 1-2 as a control prior to stimulation, while ZT 6-7 was chosen based on the dynamics of SWA response to opto-TrkB activation shown in the above-mentioned experiments (i.e., an hour where significantly high local SWA levels were expected in response to stimulation). We examined the spiking profile of individual computer-sorted single units and observed a local sleep-specific increase in the neuronal firing rate after opto-TrkB stimulation in comparison to the contralateral hemisphere (Figures 2H, 2I, and S5B). At the network level (represented by all units detected by a tetrode), we found a significant increase in neuronal discharge during NREM sleep ON periods (Figure 2J). This enhanced neuronal recruitment during ON periods has been previously reported to correlate with elevated levels of sleep pressure.[13,18] Thus, BDNF/TrkB signaling in L5 pyramidal neurons determines spiking activity during ON periods to favor local sleep SWs.

Next, we asked whether BDNF/TrkB's ability to modulate neuronal excitability[56] per se might directly explain BDNF/TrkB effects on local sleep SWA. Therefore, we uni-hemispherically targeted the expression of the excitatory hM3Dq[57] DREADD (designer receptors exclusively activated by designer drugs) to the somatosensory cortex of WT mice using stereotactic injection of *hSyn1-hM3D(Gq)-mCherry* AAV5 or *hSyn1-mCherry* AAV5 (control; Figure S6, see STAR Methods). We confirmed sufficient neuronal expression of hM3Dq and its ability to robustly induce neuronal firing using multi-electrode array (MEA) recordings in brain slices (Figure S6A–S6E, see STAR Methods). To explore the impact of increasing local network firing on subsequent sleep SWA, we recorded LFP signals in the vicinity of the injection site, contralateral hemisphere, and frontal sites (Figure S6F). We administered clozapine N-oxide (CNO; 2 mg/kg intraperitoneally) either at light onset (≈ZT 0) or light offset (≈ZT 12) and observed a local reduction of NREM SWA for ≈6–8 h with no subsequent rebound (Figures S6G and S6I). We further locally induced neuronal firing using optogenetic-based activation of channelrhodopsin-2 (ChR2) and observed a local reduction of SWA (1.25–4 Hz) with no noticeable rebound (see STAR Methods, Figure S7). Taken together, these experiments suggest that increasing neuronal firing intensity itself in cortical pyramidal neurons of the somatosensory cortex is insufficient to drive subsequent upregulation of local sleep SWA. Yet, it remains to be determined whether a specific firing pattern that resembles neuronal coding under physiological conditions could subsequently induce local sleep SWA.

BDNF-mediated upregulation of local sleep SWs is CREB-activity dependent

BDNF-TrkB dimerization stimulates autophosphorylation of the intracellular kinase domain of TrkB receptor leading to the recruitment of adaptor proteins, triggering 3 intracellular signaling cascades mediated by Ras-mitogen-activated protein kinase (MAPK), phosphatidylinositol 3-kinase (PI3K)-Akt, and the

phospholipase C (PLCγ)-Ca^{2+} pathway.[58] BDNF-dependent activation of those kinases' pathways ultimately converges in the modulation of transcription and translation in neurons.[59–62] However, the requirement of *de novo* transcription and protein synthesis for BDNF-related effects on long-lasting potentiation of synaptic plasticity remains controversial.[63–65] To investigate whether BDNF-dependent upregulation of local sleep SWs involves transcription and/or translation, we unilaterally implanted a cannula above the somatosensory cortex and co-infused BDNF together with the transcriptional inhibitor actinomycin D[66] or the translational blocker anisomycin.[67] Simultaneously, we recorded LFP signals from both the infusion site and the contralateral hemisphere (Figure 3A, see STAR Methods). Interestingly, co-infusion of BDNF (50 ng/mL) and actinomycin D (5 μg/mL; at ZT 0) abolished BDNF-dependent upregulation of SWA (between ZT 3 and 6), whereas co-infusion of BDNF (50 ng/mL) and anisomycin (40 μM; at ZT 0) resulted in a subsequent reduction in SWA (between ZT 3 and 6), confirming the necessity of *de novo* transcription and protein synthesis (Figure 3B).

We then aimed to investigate the transcriptional fingerprint, downstream of TrkB receptor activation, sufficient to modulate higher SWA. To do so, we analyzed RNA-seq from mouse somatosensory cortex after locally activating opto-TrkB (resulting in high SWA levels) or the control opto-ChR2 (resulting in low SWA levels). From the 15,642 transcripts that met detection thresholds in both conditions, 138 transcripts were differentially expressed ($p < 0.05$, |log2 fold change| ≥ 1), with almost 70% (95 transcripts) being upregulated after opto-TrkB compared to opto-ChR2 (Figure 3C). Reactome network analysis on upregulated transcripts showed that opto-TrkB activation induced transcripts with similar enrichment terms to those observed after sleep deprivation (Figure 3D).

To identify transcription factors responsible for the upregulation of transcripts under high SWA, either induced by opto-TrkB or by sleep deprivation, we compared the transcriptome data of somatosensory cortex under these conditions. Enrichment analysis of transcription factors driving transcripts upregulated after both experimental conditions increasing SWA revealed 11 transcription factor pathways significantly enriched (Fisher's exact test, FDR-adjusted $p < 0.05$) in both conditions, which we thus defined as the transcriptional signature of sleep SW regulation (Figures 3E and 3F). Notably, almost all the transcription factor signatures (10 out 11) were related to the ATF/ CREB family (hereafter referred to as CREB family; Figures 3E and 3F). Specifically, we observed that opto-TrkB as well as sleep deprivation induces an upregulation of the CREB family-related factor *Creb3L2* transcripts and a downregulation of the negative regulator *Crebrf* (Figure 3H). Indeed, opto-TrkB led to significant upregulation of neuronal activity-dependent immediate-early genes such as Arc[68,69] and NPAS4,[70] ranking among our top 20 differentially expressed transcripts (Figure 3G). Moreover, our data revealed the upregulation of a total of 13 genes (*Adamts1*, *Cort*, *Dusp1*, *Egr1*, *Egr2*, *Fos*, *Fosb*, *Fosl1*, *Gpr3*, *Inhbe*, *Lif*, *Midn*, and *Nr4a1*) that were previously characterized to contain conserved CRE sequences (CREs) in the promoter region.[71] Collectively, these findings suggest that CREB family-dependent transcriptional activity mediates elevated cortical SWA levels triggered by BDNF/TrkB.

To investigate this, we unilaterally implanted a cannula above the somatosensory cortex and co-infused the CREB inhibitor 666-15[72,73] with BDNF while recording LFP signals from both the infusion site and contralateral hemisphere (Figure 3I, see STAR Methods). Notably, co-infusion of BDNF (50 ng/mL) and 666-15 (100 μM; at ZT 0) abolished the upregulation of local sleep SWs induced by BDNF (Figure 3I). We further investigated the impact of inhibiting CREB during activation of opto-TrkB on local SWA. To assess this, we stereotactically injected *mCaM-KIIa-opto-TrkB-HA* AAV5 into the somatosensory cortex of WT mice and implanted an optical fiber above L5 cortex while simultaneously recording the LFP signal from the injection site and contralateral hemisphere (Figures 3J and 3K, see STAR

Figure 3. BDNF-mediated upregulation of local sleep SWs is CREB activity dependent

(A) Schematic of the experimental strategy.

(B) Boxplot (left) of SWA (between ZT 3 and 6) after co-infusion of BDNF (50 ng/mL) + actinomycin D (5 μg/mL) at ZT 0 as outlined on top row (n = 8, d = −0.5). Identical plot (right) for co-infusion of BDNF + anisomycin (40 μM; n = 6, d = −1.4; paired Student's t test).

(C) Schematic and timeline (top row) of the experimental procedure for the transcriptome comparison between opto-TrkB-stimulated and opo-ChR2-stimulated conditions. Horizontal bar plot (bottom row) showing the number of significantly upregulated and downregulated transcripts (n = 5 mice for opto-TrkB and 3 mice for opo-ChR2).

(D) Reactome subnetworks of the upregulated transcripts and enriched signaling pathways (top 5 pathways).

(E) Pie plots (left) of significantly enriched transcription factor terms in case of sleep deprivation vs. sleep (top, 30 terms) and for opto-TrkB vs. ChR2 (bottom, 12 terms). Red-colored pie piece represents the enriched TF terms that are overlapping between the 2 conditions.

(F) The 11 commonly enriched TF terms represented as bubble plot (left: sleep deprivation vs. sleep, right: opto-TrkB vs. ChR2). Bubble size represents the number of significant genes within cluster, bubble color reflects fold enrichment, and x axis −log10 of the FDR-adjusted p value.

(G) Heatmap for the log2 normalized counts of top 20 DEGs for opto-TrkB vs. opto-ChR2 comparison (unpaired Student's t test $p < 0.05$, log2 fold change ≥ 1).

(H) Quantification (left) of *Creb3L2* (left, d = 1.7) and *Crebrf* (right, d = −1.5) transcripts in opto-TrkB vs. opto-ChR2 conditions (unpaired Student's t test [one-tailed]). Quantification (right) of *Creb3L2* (left, d = 2.5) and *Crebrf* (right, d = −1.5) transcripts in sleep deprivation vs. sleep conditions for the same transcriptome experiment in Figures 1A–1G (respectively: unpaired Student's t test [one-tailed], and Wilcoxon rank-sum test [one -tailed]).

(I) Schematic (left) of the experimental strategy. SWA (middle) (ZT 3–6) after co-infusion of BDNF (50 ng/mL) + 666-15 (100 μM) at ZT 0 as outlined on the top row. Power spectrum (right) during NREM sleep (ZT 3–6; n = 4, paired Student's t test).
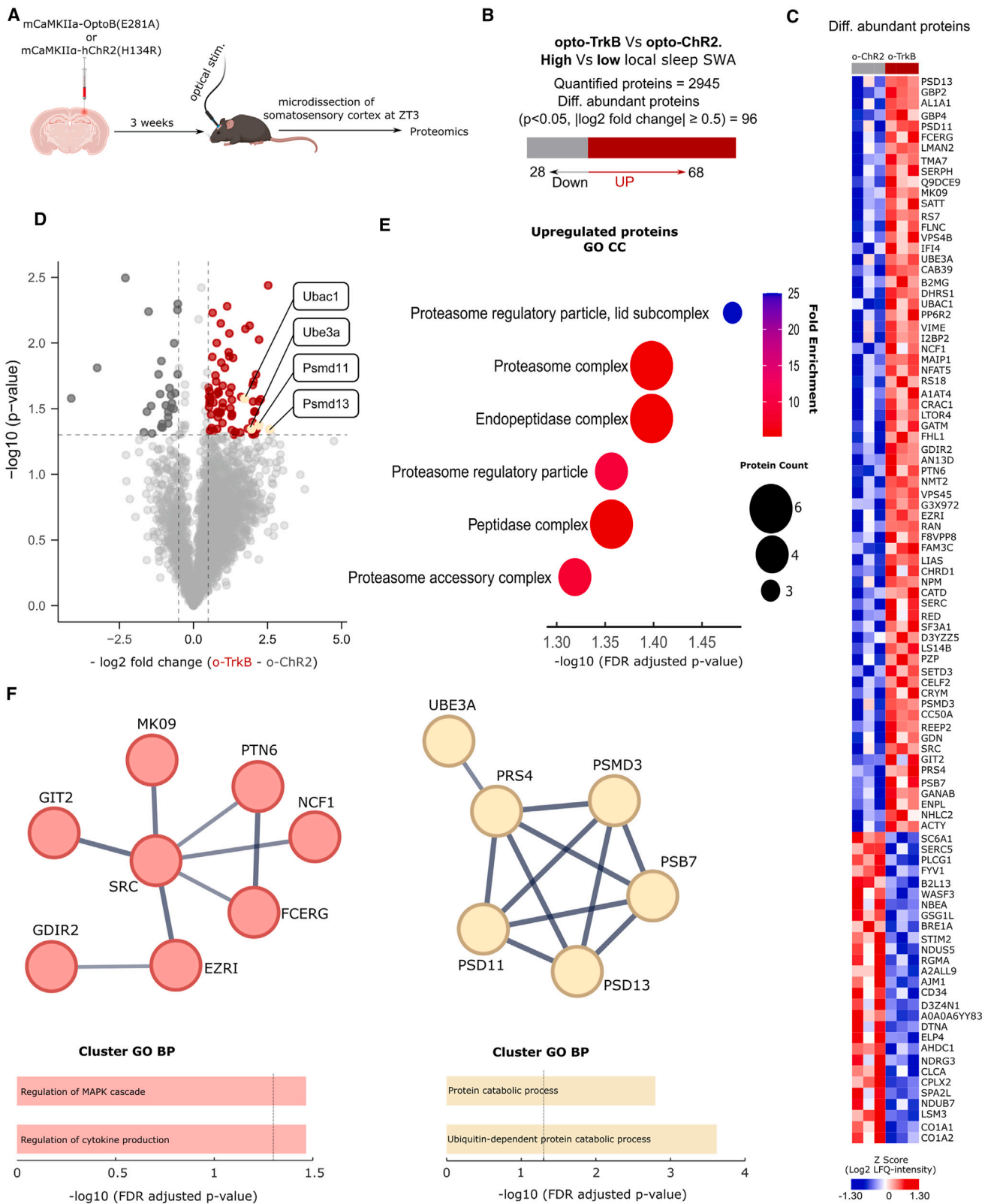
(J) Schematic for LFP electrode coupled to an infusion cannula and an optrode to study the effect of 666-15 infusion on opto-TrkB-induced local sleep SWA.

(K) The experiment timeline.

(L) SWA (between ZT 3 and 6) after vehicle injection (ZT 0) + optical stimulation (ZT 0–2) as outlined on top row (paired Student's t test, d = 1.6).

(M) SWA time course plot in response to 666-15 injection (ZT 0) + optical stimulation (ZT 0–2; n = 4, "REML").

(N) Quantification of SWA (between ZT 3 and 6; paired Student's t test, d = −5.1). See also Figure S8.

A

mCaMKIIa-OptoB(E281A)
or
mCaMKIIa-hChR2(H134R)

optical stim.

3 weeks → microdissection of somatosensory cortex at ZT3 → Proteomics

B

opto-TrkB Vs opto-ChR2.
High Vs low local sleep SWA
Quantified proteins = 2945
Diff. abundant proteins
(p<0.05, |log2 fold change| ≥ 0.5) = 96

28 ← Down   UP → 68

C

Diff. abundant proteins

o-ChR2 o-TrkB

PSD13, GBP2, AL1A1, GBP4, PSD11, FCERG, LMAN2, TMA7, SERPH, Q9DCE9, MK09, SATT, RS7, FLNC, VPS4B, IFI4, UBE3A, CAB39, B2MG, DHRS1, UBAC1, PP6R2, VIME, I2BP2, NCF1, MAIP1, NFAT5, RS18, A1AT4, CRAC1, LTOR4, GATM, FHL1, GDIR2, AN13D, PTN6, NMT2, VPS45, G3X972, EZRI, RAN, F8VPP8, FAM3C, LIAS, CHRD1, NPM, CATD, SERC, RED, SF3A1, D3YZZ5, LS14B, PZP, SETD3, CELF2, CRYM, PSMD3, CC50A, REEP2, GDN, SRC, GIT2, PRS4, PSB7, GANAB, ENPL, NHLC2, ACTY, SC6A1, SERC5, PLCG1, FYV1, B2L13, WASF3, NBEA, GSG1L, BRE1A, STIM2, NDUS5, RGMA, A2ALL9, AJM1, CD34, D3Z4N1, A0A0A6YY83, DTNA, ELP4, AHDC1, NDRG3, CLCA, CPLX2, SPA2L, NDUB7, LSM3, CO1A1, CO1A2

Z Score
(Log2 LFQ-intensity)
-1.30   0   1.30

D

Ubac1
Ube3a
Psmd11
Psmd13

- log2 fold change (o-TrkB - o-ChR2)

E

Upregulated proteins
GO CC

Proteasome regulatory particle, lid subcomplex
Proteasome complex
Endopeptidase complex
Proteasome regulatory particle
Peptidase complex
Proteasome accessory complex

Fold Enrichment: 25, 20, 15, 10

Protein Count: 6, 4, 3

-log10 (FDR adjusted p-value)

F

MK09, PTN6, GIT2, NCF1, SRC, FCERG, GDIR2, EZRI

UBE3A, PRS4, PSMD3, PSB7, PSD11, PSD13

Cluster GO BP

Regulation of MAPK cascade
Regulation of cytokine production

-log10 (FDR adjusted p-value)

Cluster GO BP

Protein catabolic process
Ubiquitin-dependent protein catabolic process

-log10 (FDR adjusted p-value)

(legend on next page)

Methods). As expected, the infusion of a vehicle (at ZT 0) during optical activation of opto-TrkB (ZT 0–2) resulted in subsequent upregulation of local SWA (ZT 3–6; Figure 3L), whereas the infusion of 666-15 (100 μM; at ZT 0) resulted in a sustained reduction of local sleep SWA (Figures 3M and 3N). Together, these findings confirm that SWA increase by the BDNF-TrkB signaling pathway requires CREB activation/function.

To further confirm the role of L5 CREB activity in regulating local sleep, we uni-hemispherically targeted the expression of rM3D(Gs) DREADD to L5 of the somatosensory cortex of *Rbp4-Cre*-expressing mice and recorded LFP signals in the vicinity of the injection site and contralateral hemisphere in freely behaving mice (Figure S8, see STAR Methods). Gs-GPCR signaling activation is well established to activate adenyl cyclase, elevate cAMP levels, and ultimately activate CREB (Figure S8A). CNO administration led to a significant increase in local sleep SWA (Figure S8D), confirming the involvement of Gs-cAMP-CREB signaling and CREB-mediated transcription activation in L5 pyramidal neurons in the regulation of local sleep SWs.

Proteome signatures upon TrkB-induced local sleep SWs

As our results indicated that BDNF/TrkB-dependent induction of local sleep depends on transcription but also translation, we next investigated the proteome signatures driven by TrkB-induced local sleep SWs using quantitative proteomics.

Mass spectrometry-based quantitative proteomics of mouse somatosensory cortex, in which TrkB or ChR2 were optogenetically activated, led to the quantification (label free quantification [LFQ]) of 2,945 proteins (Figures 4A and 4B). The statistical comparison of protein abundance between the two conditions revealed that 96 proteins showed significantly different levels ($p < 0.05$, |log2 fold change| $\geq$ 0.5), 71% (68) of which were upregulated upon TrkB-mediated elevation of SWs' levels (Figures 4B–4D). Upregulated proteins showed overrepresentation of proteasome related GO-CC annotations (Gene Ontology terms related to Cellular Components category; Fisher's exact test, FDR-adjusted $p < 0.05$, $\geq$3 proteins per pathway; Figure 4E). Notably, half of the upregulated proteasome complex proteins (PSD11, PSD13, and UBE3A) are among the most upregulated, being 4 times more abundant in response to TrkB induction (Figure 4D). Protein-protein interaction networks analysis (STRING database) on significantly upregulated proteins identified 2 distinct clusters (with $\geq$6 proteins each): one cluster with proteins related to the MAPK signaling pathway, which

has been reported to be downstream of TrkB in other contexts,[74,75] and a second cluster containing proteins associated with the proteasome, ubiquitin, and protein catabolic processes (Figure 4F). Specifically, somatosensory cortex of optogenetically activated TrkB showed significantly higher levels of components of E3 ubiquitin-protein ligase complex (UBAC1 and UBE3A) that plays a key role in histone modifications and associated epigenetic control of transcription,[76] robustness of the circadian clock,[77] and stability of sleep-wake cycles.[78] Indeed, ubiquitin and proteasome system activity has been previously documented to undergo alterations in response to BDNF, playing a decisive role in mediating its effects.[61,79] Our proteomics data reveal that BDNF-TrkB activation in mouse cortex leads to an increased abundance of proteosome-related proteins, suggesting a role for protein degradation in the induction of SWs, similarly to what has been reported in BDNF-induced synaptic plasticity.[80–82] Our data are also in line with reports implicating ubiquitin and proteasome system-mediated degradation of synaptic proteins in the regulation of sleep homeostasis in drosophila[83–85] and rodents.[86,87]

Modeling predicts that the potentiation of net synaptic weights can regulate the prevalence of cortical SWA

We next explored the ionic and network mechanisms of sleep SWs generation using mathematical modeling. We developed a computational model mimicking a cortical network comprising excitatory pyramidal neurons and inhibitory interneurons (Figure 5A, see STAR Methods). We used validated mathematical models of individual cortical neurons, which account for many ionic currents within cortical neurons. Individually, these neurons showed either quiescence or wake-type behaviors but not slow waves.

These neurons are connected via conductance-based NMDA (N-methyl-D-aspartate), AMPA (α-amino-3-hydroxy-5-methyl-4-isoxazolepropionic acid), and GABA-A (γ-Aminobutyric acid type A) signaling models (see STAR Methods). To mimic the effects of hM3Dq DREADD activation, which increases excitatory currents within neurons, we took our network and applied a tonic excitatory current, mimicking when CNO was applied in Figure S6 (Figure 5B). While this increased the firing rates of neurons in the network (Figure 5C), it did not cause SWA (Figure 5D). The network was also not bistable because it returned to its regular firing pattern when the CNO simulation was presumably washed out. This suggested that the model accurately reflected our experimental data on the effects of increased neuronal firing rate on slow waves.

Figure 4. Proteome signatures upon TrkB-induced local sleep SWs

(A) Schematic and timeline of the experimental procedure for the proteome comparison between opto-TrkB-stimulated and opo-ChR2-stimulated conditions.

(B) Horizontal bar plot showing the number of quantified, upregulated, and downregulated proteins (n per group = 3 samples collected from 9 mice, see Star Methods).

(C) Heatmap of LFQ protein intensities from the 96 differentially abundant proteins (unpaired Student's t test $p < 0.05$, |log2 LFQ intensity fold change| $\geq$ 0.5).

(D) Volcano plot of all quantified proteins. Differentially upregulated proteins are colored in red, whereas downregulated proteins are dark-gray colored. Dashed vertical lines represent ±0.5 log2 fold change of protein LFQ intensity. Dashed horizontal line represents p value of 0.05.

(E) Enriched GO-CC terms from upregulated proteins in response to TrkB stimulation.

(F) STRING protein-protein interaction network (top row) of upregulated proteins (from C) showing 2 significant clusters with $\geq$6 proteins each. Enriched GO-BP terms (Gene Ontology terms related to Biological Process category; bottom row) on each cluster protein set are shown below in the same color as the cluster. Vertical dashed line represents significant cutoff FDR-adjusted p value of 0.05.
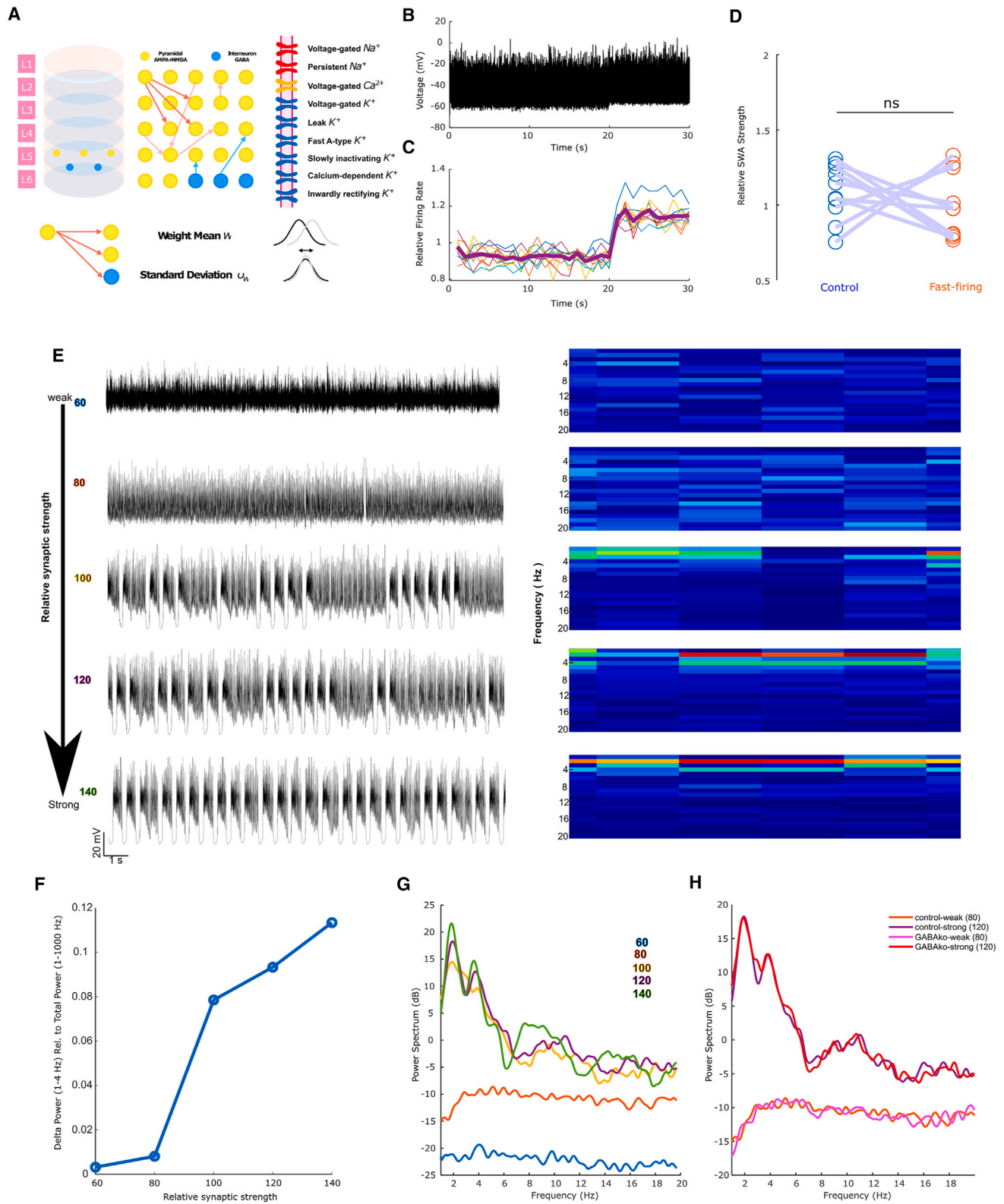
(legend on next page)

The BDNF-TrkB-CREB axis has been proven to play a critical role in memory and learning, and that role has primarily been attributed to the potentiation of synaptic plasticity.[88–91] We hypothesized that BDNF-dependent upregulation of SWs might also be due to increases in synaptic weights. This was suggested by our experimental data showing a steeper slope to UP and DOWN states indicating a greater network synchrony and synaptic plasticity with BDNF-TrkB activation. When we increased synaptic strengths in our network, mimicking the effects of upregulating BDNF or TrkB activation, we found that slow waves emerged in the network (Figures 5E and 5F). Our experimental data also suggested that excitatory pyramidal neurons mediate this increase in SWA. Similarly, when we removed GABA signaling in our network, no effect on the increased SWA was found (Figures 5G and 5H). The modeling data show a potential role of synaptic strength on sleep SWs and indicate that BDNF-mediated SWA might reflect a scenario of enhanced synaptic plasticity within a local network.

DISCUSSION

Although research on the molecular mechanisms underlying the use-dependent regulation of local SWA remains in its early stages, James Krueger and Ferenc Obal Jr. already in the 90s[26] proposed a theory to explain the mechanistic origin of local sleep. They stated that network cellular activity during wakefulness induces the production of substances/sleep factors such as the synthesis of specific ion channels or molecules critical for synaptic efficacy. These activity-dependent substances can, in turn, alter the input-output relationship within and between neuronal groups, eventually leading to modulation of their own neuronal activity and a temporary local disjunctive status in the affected neuronal group, which is denoted as "local sleep" state. In the following years, they further provided series of studies to establish a clear role for neurotrophins (e.g., BDNF,[92] nerve growth factor [NGF],[93] neurotrophin 3 [NT-3],[94] and NT-4[94]) as regulatory sleep substances. These activity-dependent molecules play a crucial role in modulating synaptic plasticity and promoting sleep when infused into the brain.[95–98] Consistent with this, our transcriptome signature of elevated sleep pressure also showed higher levels of BDNF and NTRK signaling as well as NGF-stimulated transcription (see Figure 1).

Conserved across mammalian species, four neurotrophins have been characterized: NGF, BDNF, NT-3, and NT-4.[99] They signal through binding to two types of cell surface receptor: p75NTR and NTRKs. While they equally bind with low affinity

to p75NTR, they exhibit high affinity and more selective binding to NTRKs: NGF binds to TrkA, and BDNF and NT-4 bind to TrkB, whereas NT-3 binds to TrkC and to lesser extent to TrkB. In this study, we focused on elucidating specifically how cortical BDNF levels, via the activation of TrkB receptor, regulate local sleep SWA. Interestingly, the intracerebroventricular (ICV) infusion of NT-4 and NT-3 in rabbits promoted sleep but did not increase SWA.[94] While this may raise the notion that TrkB-dependent regulation of local sleep could be exclusive to its activation by BDNF, it cannot completely rule out the contribution of cortical NT-4 or NT-3/TrkB interaction in regulating SWA, given the untargeted ICV approach used in the study. It thus remains elusive whether and how the other TrkB ligands (NT-4 and NT-3) regulate local SWA. Future experiments could potentially target their infusion into cortex to address their role in SWA control.

CREB activity is necessary for BDNF-dependent upregulation of local sleep SWs. CREB activation involves phosphorylation that could be mediated by various signal transduction pathways, including cAMP/PKA,[100] CAMKI/CAMKII and CAMKIV,[101,102] and MAPK/Erk/Rsk.[103,104] As our quantitative proteomics data show that TrkB activation, in contrast to neuronal firing, specifically leads to an upregulation of the MAPK signaling pathway (Figure 4F), we propose that BDNF-TrkB signaling leads to CREB phosphorylation, and thus activation, via the MAPK/Erk/Rsk cascade.

CREB family-driven transcription of synaptic plasticity-related genes (e.g., *Arc*) has been shown to be essential for BDNF-dependent synaptic plasticity responses such as long-lasting potentiation of synaptic transmission.[105,106] Locally, CREB has also been shown to be upregulated and required for unilateral whisker-dependent plasticity in barrel cortex,[107,108] in line with the slight increase in cortical CREB binding protein levels we observed in SD mice (Figure S9). Furthermore, it has been reported that cortical CREB phosphorylation is reduced during sleep, induced during wakefulness, and upregulated after sleep deprivation in rats.[28] Mice lacking CREB in forebrain excitatory neurons were unable to sustain consolidated periods of wakefulness, suggesting a potential role for CREB in maintaining cortical arousal.[109] In brief, our findings are consistent with previous research, providing corroborating evidence for the involvement of CREB in the control of the sleep/wake landscape and proposing a contribution of CREB in regulating SWA, at least locally.

The CREB-encoding gene, through alternative splicing, produces different proteins isoforms including activators and repressors of gene transcription.[110] Repressors lack transcription

Figure 5. Modeling predicts that potentiation of net synaptic weights can regulate the prevalence of cortical SWs
(A) Schematic for the computational model.
(B) The LFP trace of the network, where an applied current was injected from t = 20 to t = 30 s.
(C) Traces of relative firing rate of 10 sample neurons, where the purple thick line is the average.
(D) Comparison of the relative SWA strength of 10 neurons during control and with applied current (fast firing). Each dot represents a neuron, paired Student's t test.
(E) LFP raw traces (left) showing an increase in slow wave prevalence upon increasing net synaptic weights in our network (top to bottom). The corresponding spectrograms are shown (right).
(F) SWA in response to increased network net synaptic weights.
(G) Line plot representations of spectrograms provided in (E). Note the increase in delta power upon increasing net synaptic weights.
(H) Power spectra showing no effect on the increased SWA in a network that lacks GABA signaling. Note the similarity in power distribution between control and GABA knockout conditions.

activation domains but possess DNA binding and dimerization domains. These proteins form inactive heterodimers with the activator CREB (referred to as CREB), hindering its access to the CREs. In addition to CREB phosphorylation, transcription induction by CREB requires the removal of repressor-mediated blockade. These repressors are substrates for degradation through the ubiquitin/proteasome pathway. And this degradation process is crucial for CREB-mediated gene transcription and is associated with long-term facilitation.[111] Thus, the simultaneous upregulation of *Creb3L2* and downregulation of the negative regulator *Crebrf* in response to opto-TrkB activation, along with ubiquitin/proteasome upregulation, may cooperatively enhance CREB-mediated transcription of synaptic plasticity-related genes.

LFP is widely shaped by a spatial and temporal summation of the respective current sources, primarily post-synaptic potentials, surrounding the electrode area.[112] Synchrony among neurons strongly influences EEG amplitude, where higher synchrony corresponds to higher EEG amplitude.[112,113] We induced local network firing using chemogenetics (i.e., hM3Dq) and optogenetics (i.e., ChR2), both resulting in a reduction of LFP delta power. Upon induction of neuronal firing, we locally enforced firing in a defined population of neurons regardless of the network coordination state, which is mainly regulated via synaptic inputs from neighboring cortical networks and subcortical structures. This conflict between an artificial input source and synapse-to-network input may perturb neuronal synchrony leading to the observed reduction in LFP power.[114] Yet, the precise contribution of neuronal firing and/or synchrony on sleep SWs' dynamics remains to be further investigated. Surprisingly, this increase in firing content was not sufficient to elicit compensatory changes in local sleep SWs (i.e., no subsequent SWs rebound), indicating that the increase in cortical neurons discharge rate alone may not be the primary factor causing the accumulation of local sleep SWs. Nevertheless, this doesn't rule out the potential contribution of specific firing patterns that are mimicking physiological cortical activity during local sleep inducing-tasks.

Sleep delta band consists of two types of delta waves: a faster component ($\delta2$: $\approx$2.25–4 Hz), sensitive to thalamic manipulations,[115,116] and a slower population ($\delta1$: $\approx$0.75–1.5 Hz) that rather more likely reflects cortical slow oscillatory activities.[20,115,117] We observed that both $\delta1$ and $\delta2$ bands increased in response to local opto-TrkB activation, with a larger effect size in $\delta1$, reflecting sensitivity to cortical manipulation as anticipated (Figures S5A and S4).

More than 30 years ago, BDNF mRNA was found to be highly enriched in the cortex of mouse brain.[118] BDNF expression is restricted to pyramidal neurons,[119] while its receptor TrkB was found in both pyramidal neurons and interneurons, making both types of neurons responsive to BDNF.[120,121] In the somatosensory cortex, BDNF is expressed across cortical layers 2–6 and absent in layer 1.[122] Layers 5–6 exhibit the highest BDNF levels, while layer 4 shows very low levels (almost undetectable).[119,122,123] TrkB, however, is detectable in all layers, with L5 showing the densest expression.[124,125] Consistent with other studies showing that cortical layer 5 predominantly expresses higher SWs' amplitude than superficial layers,[126,127] TrkB activa-

tion on cortical layer 5 resulted in subsequent upregulation of SWA, while it did not on superficial layers (L2 and L3) as well as L6. Together, this indicates a leading role of BDNF-TrkB signaling in cortical L5 pyramidal neurons in catalyzing the buildup of local use-dependent sleep SWs.

The effects of BDNF on LTP have mainly been attributed to posttranslational modifications of existing proteins and their trafficking at synapses to facilitate early LTP (E-LTP)[128–130] and to the induction of *de novo* transcriptional and translational activities, leading to late LTP (L-LTP).[130,131] Concomitantly, BDNF transiently inhibits ubiquitin/proteasomes activity, which in turn leads to an increase of key functional proteins at synapses during E-LTP.[81] On the other hand, ubiquitin/proteasomes activity, via calibrating protein turnover, was shown to be instrumental to ensure proper synaptic protein homeostasis that is critical for facilitation of BDNF-dependent L-LTP.[81] This is in agreement with our proteomics data showing noticeable upregulation of proteasome-related proteins following 3 h of TrkB activation. Interestingly, BDNF-TrkB effects on local sleep SWs share a striking pattern of similarity with BDNF-mediated L-LTP including a delayed response to TrkB activation (2–3 h to observe SWs upregulation), a dependence on *de novo* transcription and protein synthesis, a reliance on CREB family activity, and the activation of proteasome complex. Thus, local sleep SWs could potentially be a consequence of local experience-dependent L-LTP occurring during wakefulness and thus share molecular features.

This is suggested by our mathematical modeling work where increases in excitatory, but not inhibitory, signaling in a local cortical network can trigger SWA. While existing models discuss how BDNF can change a single synapse activity,[132,133] our proposed model addresses the effect of BDNF on a network level. Local SWA occurrences have been treated as an indicator of level of cognitive fatigue,[134,135] where overtaxing local networks through exhausting or repetitive tasks can cause an increase of local SWA at different brain regions. Therefore, an interesting future perspective is to study how BDNF-induced local SWA is coordinated throughout the brain network. Furthermore, the model also has the potential to determine the detailed electrophysiological reason, i.e., the possible ionic and synaptic currents that are related to the BDNF-induced SWA.

Limitations of the study

We acknowledge several limitations in our study. The first limitation is that our focus was solely on elucidating molecular mechanisms underlying local sleep without exploring their impact on global sleep SWA. Future investigations should involve ICV infusion of k252a to achieve a broader blockade of TrkB activation and examine whether it could attenuate global increase of SWA following sleep deprivation. A second limitation is that we have exclusively relied on pharmacological blockade experiments to demonstrate the loss of function of TrkB and CREB. Future studies should conduct conditional genetic knockout of CREB and/or selectively optogenetically activate CREB to further delve deeper into its role in regulation of sleep SWA. Future studies should also address the mechanisms for how CREB shuttles between the cytoplasm and nucleus and how

this process is influenced by BDNF/TrkB signaling and/or sleep pressure in general.

Although the model has managed to reproduce several results of the experiment, there are some limitations. We did not incorporate the layered cortical structure in our model and were not able to confirm the specific layer of neurons that is causing the increase in SWA as the experiment did. We also did not include any molecular details that could correspond to the transcriptomic data collected. Future modeling work could work in those directions to improve the model.

STAR★METHODS

Detailed methods are provided in the online version of this paper and include the following:

- KEY RESOURCES TABLE
- RESOURCE AVAILABILITY
  - Lead contact
  - Materials availability
  - Data and code availability
- EXPERIMENTAL MODEL AND STUDY PARTICIPANT DETAILS
  - Animals
- METHOD DETAILS
  - Surgeries
  - Immunofluorescence staining
  - Acute slice preparation and ex-vivo multi-electrode recordings
  - *In vivo* recordings in freely behaving mice & analysis
  - Transcriptomics
  - Proteomics
  - Computational model and simulation
  - Plotting
- QUANTIFICATION AND STATISTICAL ANALYSIS

SUPPLEMENTAL INFORMATION

Supplemental information can be found online at https://doi.org/10.1016/j. celrep.2024.114500.

AUTHOR CONTRIBUTIONS

S.A.B. and W.E. conceptualized the project. W.E., A.R.A., D.B.F., and M.S.R. wrote the manuscript. S.A.B. and W.E. designed omics experiments. W.E. performed transcriptomics experiment under supervision of S.A.B. W.E. and F.P.K. performed proteome experiments, and W.E. and F.P.K. analyzed proteome under supervision of M.S.R. A.R.-A. assisted with proteome preparation. *In vivo* EEG recordings and analysis were done by W.E. under supervision of S.A.B. *In vitro* electrophysiology and analysis were done by S.P.-F. and W.E. A.R.A., W.E., and S.A.B. designed the *in vivo* tetrode experiments, S.S. performed the experiment with guidance of I.B., and W.E. and S.S. performed analysis under supervision of S.A.B. W.D.H. provided the opto-TrkB adeno-associated viruses. P.B. and F.H. contributed mice. G.S. performed modeling under the supervision of D.B.F.

REFERENCES

1. Massimini, M., Huber, R., Ferrarelli, F., Hill, S., and Tononi, G. (2004). The sleep slow oscillation as a traveling wave. J. Neurosci. *24*, 6862–6870. https://doi.org/10.1523/JNEUROSCI.1318-04.2004.

2. Borbély, A.A. (1982). A two process model of sleep regulation. Hum. Neurobiol. *1*, 195–204.

3. Achermann, P., and Borbély, A.A. (2003). Mathematical models of sleep regulation. Front. Biosci. *8*, s683–s693. https://doi.org/10.2741/1064.

4. Borbély, A.A., and Achermann, P. (1999). Sleep homeostasis and models of sleep regulation. J. Biol. Rhythm. *14*, 557–568. https://doi.org/10.1177/074873099129000894.

5. Franken, P. (2007). The Quality of Waking and Process S. Sleep *30*, 126–127. https://doi.org/10.1093/sleep/30.2.126.

6. Finelli, L.A., Achermann, P., and Borbély, A.A. (2001). Individual 'Fingerprints' in Human Sleep EEG Topography. Neuropsychopharmacology *25*, S57–S62. https://doi.org/10.1016/S0893-133X(01)00320-7.

7. Rattenborg, N.C., Amlaner, C.J., and Lima, S.L. (2000). Behavioral, neurophysiological and evolutionary perspectives on unihemispheric sleep. Neurosci. Biobehav. Rev. *24*, 817–842. https://doi.org/10.1016/S0149-7634(00)00039-7.

8. Mukhametov, L.M., Supin, A.Y., and Polyakova, I.G. (1977). Interhemispheric asymmetry of the electroencephalographic sleep patterns in dolphins. Brain Res. *134*, 581–584. https://doi.org/10.1016/0006-8993(77)90835-6.

9. Rattenborg, N.C., Voirin, B., Cruz, S.M., Tisdale, R., Dell'Omo, G., Lipp, H.-P., Wikelski, M., and Vyssotski, A.L. (2016). Evidence that birds sleep in mid-flight. Nat. Commun. *7*, 12468. https://doi.org/10.1038/ncomms12468.

10. Kattler, H., Dijk, D.-J., and Borbély, A.A. (1994). Effect of unilateral somatosensory stimulation prior to sleep on the sleep EEG in humans. J. Sleep Res. *3*, 159–164. https://doi.org/10.1111/j.1365-2869.1994.tb00123.x.

11. Huber, R., Felice Ghilardi, M., Massimini, M., and Tononi, G. (2004). Local sleep and learning. Nature *430*, 78–81. https://doi.org/10.1038/nature02663.

12. Vyazovskiy, V.V., Borbély, A.A., and Tobler, I. (2000). Unilateral vibrissae stimulation during waking induces interhemispheric EEG asymmetry during subsequent sleep in the rat. J. Sleep Res. *9*, 367–371. https://doi.org/10.1046/j.1365-2869.2000.00230.x.

13. Alfonsa, H., Burman, R.J., Brodersen, P.J.N., Newey, S.E., Mahfooz, K., Yamagata, T., Panayi, M.C., Bannerman, D.M., Vyazovskiy, V.V., and Akerman, C.J. (2023). Intracellular chloride regulation mediates local sleep pressure in the cortex. Nat. Neurosci. *26*, 64–78. https://doi.org/10.1038/s41593-022-01214-2.

14. Facchin, L., Schöne, C., Mensen, A., Bandarabadi, M., Pilotto, F., Saxena, S., Libourel, P.A., Bassetti, C.L.A., and Adamantidis, A.R. (2020). Slow Waves Promote Sleep-Dependent Plasticity and Functional Recovery after Stroke. J. Neurosci. *40*, 8637–8651. https://doi.org/10.1523/JNEUROSCI.0373-20.2020.

15. Desiraju, T. (1972). Discharge properties of neurons of the parietal association cortex during states of sleep and wakefulness in the monkey. Brain Res. *47*, 69–75. https://doi.org/10.1016/0006-8993(72)90252-1.

16. Hobson, J.A., and McCarley, R.W. (1971). Cortical unit activity in sleep and waking. Electroencephalogr. Clin. Neurophysiol. *30*, 97–112. https://doi.org/10.1016/0013-4694(71)90271-9.

17. Steriade, M., Timofeev, I., and Grenier, F. (2001). Natural Waking and Sleep States: A View From Inside Neocortical Neurons. J. Neurophysiol. *85*, 1969–1985. https://doi.org/10.1152/jn.2001.85.5.1969.

18. Vyazovskiy, V.V., Olcese, U., Lazimy, Y.M., Faraguna, U., Esser, S.K., Williams, J.C., Cirelli, C., and Tononi, G. (2009). Cortical firing and sleep homeostasis. Neuron *63*, 865–878. https://doi.org/10.1016/j.neuron.2009.08.024.

19. Contreras, D., and Steriade, M. (1995). Cellular basis of EEG slow rhythms: a study of dynamic corticothalamic relationships. J. Neurosci. *15*, 604–622. https://doi.org/10.1523/JNEUROSCI.15-01-00604.1995.

20. Steriade, M., Nuñez, A., and Amzica, F. (1993). Intracellular analysis of relations between the slow (< 1 Hz) neocortical oscillation and other sleep rhythms of the electroencephalogram. J. Neurosci. *13*, 3266–3283. https://doi.org/10.1523/JNEUROSCI.13-08-03266.1993.

21. Mukovski, M., Chauvette, S., Timofeev, I., and Volgushev, M. (2007). Detection of Active and Silent States in Neocortical Neurons from the Field Potential Signal during Slow-Wave Sleep. Cerebr. Cortex *17*, 400–414. https://doi.org/10.1093/cercor/bhj157.

22. Saberi-Moghadam, S., Simi, A., Setareh, H., Mikhail, C., and Tafti, M. (2018). In vitro Cortical Network Firing is Homeostatically Regulated: A Model for Sleep Regulation. Sci. Rep. *8*, 6297. https://doi.org/10.1038/s41598-018-24339-6.

23. Chen, J., Reitzen, S.D., Kohlenstein, J.B., and Gardner, E.P. (2009). Neural Representation of Hand Kinematics During Prehension in Posterior Parietal Cortex of the Macaque Monkey. J. Neurophysiol. *102*, 3310–3328. https://doi.org/10.1152/jn.90942.2008.

24. Zhu, J.J., and Connors, B.W. (1999). Intrinsic Firing Patterns and Whisker-Evoked Synaptic Responses of Neurons in the Rat Barrel Cortex. J. Neurophysiol. *81*, 1171–1183. https://doi.org/10.1152/jn.1999.81.3.1171.

25. Dooley, J.C., Glanz, R.M., Sokoloff, G., and Blumberg, M.S. (2020). Self-Generated Whisker Movements Drive State-Dependent Sensory Input to Developing Barrel Cortex. Curr. Biol. *30*, 2404–2410.e4. https://doi.org/10.1016/j.cub.2020.04.045.

26. Krueger, J.M., and Obál, F. (1993). A neuronal group theory of sleep function. J. Sleep Res. *2*, 63–69. https://doi.org/10.1111/j.1365-2869.1993.tb00064.x.

27. Tononi, G., and Cirelli, C. (2003). Sleep and synaptic homeostasis: a hypothesis. Brain Res. Bull. *62*, 143–150. https://doi.org/10.1016/j.brainresbull.2003.09.004.

28. Cirelli, C., and Tononi, G. (2000). Differential Expression of Plasticity-Related Genes in Waking and Sleep and Their Regulation by the Noradrenergic System. J. Neurosci. *20*, 9187–9194. https://doi.org/10.1523/JNEUROSCI.20-24-09187.2000.

29. Huber, R., Tononi, G., and Cirelli, C. (2007). Exploratory behavior, cortical BDNF expression, and sleep homeostasis. Sleep *30*, 129–139. https://doi.org/10.1093/sleep/30.2.129.

30. Timmusk, T., Palm, K., Metsis, M., Reintam, T., Paalme, V., Saarma, M., and Persson, H. (1993). Multiple promoters direct tissue-specific expression of the rat BDNF gene. Neuron *10*, 475–489. https://doi.org/10.1016/0896-6273(93)90335-o.

31. Aid, T., Kazantseva, A., Piirsoo, M., Palm, K., and Timmusk, T. (2007). Mouse and rat BDNF gene structure and expression revisited. J. Neurosci. Res. *85*, 525–535. https://doi.org/10.1002/jnr.21139.

32. Hill, J.L., Hardy, N.F., Jimenez, D.V., Maynard, K.R., Kardian, A.S., Pollock, C.J., Schloesser, R.J., and Martinowich, K. (2016). Loss of promoter IV-driven BDNF expression impacts oscillatory activity during sleep, sensory information processing and fear regulation. Transl. Psychiatry *6*, e873. https://doi.org/10.1038/tp.2016.153.

33. Faraguna, U., Vyazovskiy, V.V., Nelson, A.B., Tononi, G., and Cirelli, C. (2008). A Causal Role for Brain-Derived Neurotrophic Factor in the Homeostatic Regulation of Sleep. J. Neurosci. *28*, 4088–4095. https://doi.org/10.1523/JNEUROSCI.5510-07.2008.

34. Muheim, C.M., Spinnler, A., Sartorius, T., Dürr, R., Huber, R., Kabagema, C., Ruth, P., and Brown, S.A. (2019). Dynamic- and Frequency-Specific Regulation of Sleep Oscillations by Cortical Potassium Channels. Curr. Biol. *29*, 2983–2992.e3. https://doi.org/10.1016/j.cub.2019.07.056.

35. Noya, S.B., Colameo, D., Brüning, F., Spinnler, A., Mircsof, D., Opitz, L., Mann, M., Tyagarajan, S.K., Robles, M.S., and Brown, S.A. (2019). The forebrain synaptic transcriptome is organized by clocks but its proteome is driven by sleep. Science *366*, eaav2642. https://doi.org/10.1126/science.aav2642.

36. Fabregat, A., Sidiropoulos, K., Viteri, G., Forner, O., Marin-Garcia, P., Arnau, V., D'Eustachio, P., Stein, L., and Hermjakob, H. (2017). Reactome pathway analysis: a high-performance in-memory approach. BMC Bioinf. *18*, 142. https://doi.org/10.1186/s12859-017-1559-2.

37. Lee, K.S., Alvarenga, T.A., Guindalini, C., Andersen, M.L., Castro, R.M., and Tufik, S. (2009). Validation of commonly used reference genes for sleep-related gene expression studies. BMC Mol. Biol. *10*, 45. https://doi.org/10.1186/1471-2199-10-45.

38. Fujihara, H., Sei, H., Morita, Y., Ueta, Y., and Morita, K. (2003). Short-term sleep disturbance enhances brain-derived neurotrophic factor gene expression in rat hippocampus by acting as internal stressor. J. Mol. Neurosci. *21*, 223–232. https://doi.org/10.1385/JMN:21:3:223.

39. Taishi, P., Sanchez, C., Wang, Y., Fang, J., Harding, J.W., and Krueger, J.M. (2001). Conditions that affect sleep alter the expression of molecules associated with synaptic plasticity. Am. J. Physiol. Regul. Integr. Comp. Physiol. *281*, R839–R845. https://doi.org/10.1152/ajpregu.2001.281.3.R839.

40. Cirelli, C., and Tononi, G. (2000). Gene expression in the brain across the sleep-waking cycle. Brain Res. *885*, 303–321. https://doi.org/10.1016/s0006-8993(00)03008-0.

41. Hairston, I.S., Peyron, C., Denning, D.P., Ruby, N.F., Flores, J., Sapolsky, R.M., Heller, H.C., and O'Hara, B.F. (2004). Sleep Deprivation Effects on Growth Factor Expression in Neonatal Rats: A Potential Role for BDNF in the Mediation of Delta Power. J. Neurophysiol. *91*, 1586–1595. https://doi.org/10.1152/jn.00894.2003.

42. Shi, T., Jagannath, A., Dang, Q., Taylor, L., and Jagannath, A. (2023). Sex-specific regulation of the cortical transcriptome in response to sleep deprivation. Front. Neurosci. *17*, 1303727. https://doi.org/10.3389/fnins.2023.1303727.

43. Cirelli, C., Gutierrez, C.M., and Tononi, G. (2004). Extensive and Divergent Effects of Sleep and Wakefulness on Brain Gene Expression. Neuron *41*, 35–43. https://doi.org/10.1016/S0896-6273(03)00814-6.

44. Thompson, C., Wisor, J., Lee, C.-K., Pathak, S., Gerashchenko, D., Smith, K., Fischer, S., Kuan, C., Sunkin, S., Ng, L., et al. (2010). Molecular and Anatomical Signatures of Sleep Deprivation in the Mouse Brain. Front. Neurosci. *4*, 165.

45. Hall, S., Deurveilher, S., Ko, K.R., Burns, J., and Semba, K. (2017). Region-specific increases in FosB/ΔFosB immunoreactivity in the rat brain in response to chronic sleep restriction. Behav. Brain Res. *322*, 9–17. https://doi.org/10.1016/j.bbr.2017.01.024.

46. Zhu, J., Hafycz, J., Keenan, B.T., Guo, X., Pack, A., and Naidoo, N. (2020). Acute Sleep Loss Upregulates the Synaptic Scaffolding Protein, Homer1a, in Non-canonical Sleep/Wake Brain Regions, Claustrum, Piriform and Cingulate Cortices. Front. Neurosci. *14*, 188. https://doi.org/10.3389/fnins.2020.00188.

47. Franken, P., Thomason, R., Heller, H.C., and O'Hara, B.F. (2007). A non-circadian role for clock-genes in sleep homeostasis:a strain comparison. BMC Neurosci. *8*, 87. https://doi.org/10.1186/1471-2202-8-87.

48. Barbacid, M. (1994). The Trk family of neurotrophin receptors. J. Neurobiol. *25*, 1386–1403. https://doi.org/10.1002/neu.480251107.

49. Tapley, P., Lamballe, F., and Barbacid, M. (1992). K252a is a selective inhibitor of the tyrosine protein kinase activity of the trk family of oncogenes and neurotrophin receptors. Oncogene 7, 371–381.

50. Baker-Herman, T.L., Fuller, D.D., Bavis, R.W., Zabka, A.G., Golder, F.J., Doperalski, N.J., Johnson, R.A., Watters, J.J., and Mitchell, G.S. (2004). BDNF is necessary and sufficient for spinal respiratory plasticity following intermittent hypoxia. Nat. Neurosci. 7, 48–55. https://doi.org/10.1038/nn1166.

51. Hong, J., and Heo, W.D. (2020). Optogenetic Modulation of TrkB Signaling in the Mouse Brain. J. Mol. Biol. 432, 815–827. https://doi.org/10.1016/j.jmb.2020.01.010.

52. Riedner, B.A., Vyazovskiy, V.V., Huber, R., Massimini, M., Esser, S., Murphy, M., and Tononi, G. (2007). Sleep homeostasis and cortical synchronization: III. A high-density EEG study of sleep slow waves in humans. Sleep 30, 1643–1657. https://doi.org/10.1093/sleep/30.12.1643.

53. Harris, J.A., Hirokawa, K.E., Sorensen, S.A., Gu, H., Mills, M., Ng, L.L., Bohn, P., Mortrud, M., Ouellette, B., Kidney, J., et al. (2014). Anatomical characterization of Cre driver mice for neural circuit mapping and manipulation. Front. Neural Circ. 8, 76.

54. Husse, J., Zhou, X., Shostak, A., Oster, H., and Eichele, G. (2011). Synaptotagmin10-Cre, a Driver to Disrupt Clock Genes in the SCN. J. Biol. Rhythm. 26, 379–389. https://doi.org/10.1177/0748730411415363.

55. Smith, M.A., Choudhury, A.I., Glegola, J.A., Viskaitis, P., Irvine, E.E., Silva, P.C.C. de C., Khadayate, S., Zeilhofer, H.U., and Withers, D.J. (2020). Extrahypothalamic GABAergic nociceptin–expressing neurons regulate AgRP neuron activity to control feeding behavior. J. Clin. Invest. 130, 126–142. https://doi.org/10.1172/JCI130340.

56. Desai, N.S., Rutherford, L.C., and Turrigiano, G.G. (1999). BDNF Regulates the Intrinsic Excitability of Cortical Neurons. Learn. Mem. 6, 284–291.

57. Roth, B.L. (2016). DREADDs for Neuroscientists. Neuron 89, 683–694. https://doi.org/10.1016/j.neuron.2016.01.040.

58. Minichiello, L. (2009). TrkB signalling pathways in LTP and learning. Nat. Rev. Neurosci. 10, 850–860. https://doi.org/10.1038/nrn2738.

59. Takei, N., Kawamura, M., Hara, K., Yonezawa, K., and Nawa, H. (2001). Brain-derived Neurotrophic Factor Enhances Neuronal Translation by Activating Multiple Initiation Processes: COMPARISON WITH THE EFFECTS OF INSULIN. J. Biol. Chem. 276, 42818–42825. https://doi.org/10.1074/jbc.M103237200.

60. Schratt, G.M., Nigh, E.A., Chen, W.G., Hu, L., and Greenberg, M.E. (2004). BDNF Regulates the Translation of a Select Group of mRNAs by a Mammalian Target of Rapamycin-Phosphatidylinositol 3-Kinase-Dependent Pathway during Neuronal Development. J. Neurosci. 24, 7366–7377. https://doi.org/10.1523/JNEUROSCI.1739-04.2004.

61. Manadas, B., Santos, A.R., Szabadfi, K., Gomes, J.R., Garbis, S.D., Fountoulakis, M., and Duarte, C.B. (2009). BDNF-Induced Changes in the Expression of the Translation Machinery in Hippocampal Neurons: Protein Levels and Dendritic mRNA. J. Proteome Res. 8, 4536–4552. https://doi.org/10.1021/pr900366x.

62. Reichardt, L.F. (2006). Neurotrophin-regulated signalling pathways. Philos. Trans. R. Soc. Lond. B Biol. Sci. 361, 1545–1564. https://doi.org/10.1098/rstb.2006.1894.

63. Mei, F., Nagappan, G., Ke, Y., Sacktor, T.C., and Lu, B. (2011). BDNF Facilitates L-LTP Maintenance in the Absence of Protein Synthesis through PKMζ. PLoS One 6, e21568. https://doi.org/10.1371/journal.pone.0021568.

64. Kang, H., and Schuman, E.M. (1996). A Requirement for Local Protein Synthesis in Neurotrophin-Induced Hippocampal Synaptic Plasticity. Science 273, 1402–1406. https://doi.org/10.1126/science.273.5280.1402.

65. Pang, P.T., Nagappan, G., Guo, W., and Lu, B. (2016). Extracellular and intracellular cleavages of proBDNF required at two distinct stages of late-phase LTP. Npj Sci. Learn. 1, 16003–16010. https://doi.org/10.1038/npjscilearn.2016.3.

66. Cassé, C., Giannoni, F., Nguyen, V.T., Dubois, M.-F., and Bensaude, O. (1999). The Transcriptional Inhibitors, Actinomycin D and α-Amanitin, Activate the HIV-1 Promoter and Favor Phosphorylation of the RNA Polymerase II C-terminal Domain. J. Biol. Chem. 274, 16097–16106. https://doi.org/10.1074/jbc.274.23.16097.

67. Iordanov, M.S., Pribnow, D., Magun, J.L., Dinh, T.H., Pearson, J.A., Chen, S.L., and Magun, B.E. (1997). Ribotoxic stress response: activation of the stress-activated protein kinase JNK1 by inhibitors of the peptidyl transferase reaction and by sequence-specific RNA damage to the alpha-sarcin/ricin loop in the 28S rRNA. Mol. Cell Biol. 17, 3373–3381. https://doi.org/10.1128/MCB.17.6.3373.

68. Korb, E., and Finkbeiner, S. (2011). Arc in synaptic plasticity: from gene to behavior. Trends Neurosci. 34, 591–598. https://doi.org/10.1016/j.tins.2011.08.007.

69. Shepherd, J.D., and Bear, M.F. (2011). New views of Arc, a master regulator of synaptic plasticity. Nat. Neurosci. 14, 279–284. https://doi.org/10.1038/nn.2708.

70. Sun, X., and Lin, Y. (2016). Npas4: Linking Neuronal Activity to Memory. Trends Neurosci. 39, 264–275. https://doi.org/10.1016/j.tins.2016.02.003.

71. Zhang, X., Odom, D.T., Koo, S.-H., Conkright, M.D., Canettieri, G., Best, J., Chen, H., Jenner, R., Herbolsheimer, E., Jacobsen, E., et al. (2005). Genome-wide analysis of cAMP-response element binding protein occupancy, phosphorylation, and target gene activation in human tissues. Proc. Natl. Acad. Sci. USA 102, 4459–4464. https://doi.org/10.1073/pnas.0501076102.

72. Xie, F., Fan, Q., Li, B.X., and Xiao, X. (2019). Discovery of a Synergistic Inhibitor of cAMP-Response Element Binding Protein (CREB)-Mediated Gene Transcription with 666-15. J. Med. Chem. 62, 11423–11429. https://doi.org/10.1021/acs.jmedchem.9b01207.

73. Li, B.X., Gardner, R., Xue, C., Qian, D.Z., Xie, F., Thomas, G., Kazmierczak, S.C., Habecker, B.A., and Xiao, X. (2016). Systemic Inhibition of CREB is Well-tolerated in vivo. Sci. Rep. 6, 34513. https://doi.org/10.1038/srep34513.

74. Revest, J.M., Le Roux, A., Roullot-Lacarrière, V., Kaouane, N., Vallée, M., Kasanetz, F., Rougé-Pont, F., Tronche, F., Desmedt, A., and Piazza, P.V. (2014). BDNF-TrkB signaling through Erk1/2 MAPK phosphorylation mediates the enhancement of fear memory induced by glucocorticoids. Mol. Psychiatry 19, 1001–1009. https://doi.org/10.1038/mp.2013.134.

75. Hua, Z., Gu, X., Dong, Y., Tan, F., Liu, Z., Thiele, C.J., and Li, Z. (2016). PI3K and MAPK pathways mediate the BDNF/TrkB-increased metastasis in neuroblastoma. Tumour Biol. 37, 16227–16236. https://doi.org/10.1007/s13277-016-5433-z.

76. Wang, J., Qiu, Z., and Wu, Y. (2018). Ubiquitin Regulation: The Histone Modifying Enzyme's Story. Cells 7, 118. https://doi.org/10.3390/cells7090118.

77. Stojkovic, K., Wing, S.S., and Cermakian, N. (2014). A central role for ubiquitination within a circadian clock protein modification code. Front. Mol. Neurosci. 7, 69.

78. D'Alessandro, M., Beesley, S., Kim, J.K., Jones, Z., Chen, R., Wi, J., Kyle, K., Vera, D., Pagano, M., Nowakowski, R., and Lee, C. (2017). Stability of Wake-Sleep Cycles Requires Robust Degradation of the PERIOD Protein. Curr. Biol. 27, 3454–3467.e8. https://doi.org/10.1016/j.cub.2017.10.014.

79. Liao, L., Pilotte, J., Xu, T., Wong, C.C.L., Edelman, G.M., Vanderklish, P., and Yates, J.R. (2007). BDNF Induces Widespread Changes in Synaptic Protein Content and Up-Regulates Components of the Translation Machinery: An Analysis Using High-Throughput Proteomics. J. Proteome Res. 6, 1059–1071. https://doi.org/10.1021/pr060358f.

80. Leal, G., Afonso, P.M., Salazar, I.L., and Duarte, C.B. (2015). Regulation of hippocampal synaptic plasticity by BDNF. Brain Res. 1621, 82–101. https://doi.org/10.1016/j.brainres.2014.10.019.

81. Santos, A.R., Mele, M., Vaz, S.H., Kellermayer, B., Grimaldi, M., Colino-Oliveira, M., Rombo, D.M., Comprido, D., Sebastião, A.M., and Duarte, C.B. (2015). Differential Role of the Proteasome in the Early and Late Phases of BDNF-Induced Facilitation of LTP. J. Neurosci. *35*, 3319–3329. https://doi.org/10.1523/JNEUROSCI.4521-14.2015.

82. Guntupalli, S., Park, P., Han, D.H., Zhang, L., Yong, X.L.H., Ringuet, M., Blackmore, D.G., Jhaveri, D.J., Koentgen, F., Widagdo, J., et al. (2023). Ubiquitination of the GluA1 Subunit of AMPA Receptors Is Required for Synaptic Plasticity, Memory, and Cognitive Flexibility. J. Neurosci. *43*, 5448–5457. https://doi.org/10.1523/JNEUROSCI.1542-22.2023.

83. Ukita, Y., Okumura, M., and Chihara, T. (2022). Ubiquitin proteasome system in circadian rhythm and sleep homeostasis: Lessons from Drosophila. Gene Cell. *27*, 381–391. https://doi.org/10.1111/gtc.12935.

84. Li, Q., Kellner, D.A., Hatch, H.A.M., Yumita, T., Sanchez, S., Machold, R.P., Frank, C.A., and Stavropoulos, N. (2017). Conserved properties of Drosophila Insomniac link sleep regulation and synaptic function. PLoS Genet. *13*, e1006815. https://doi.org/10.1371/journal.pgen.1006815.

85. Stavropoulos, N., and Young, M.W. (2011). insomniac and Cullin-3 Regulate Sleep and Wakefulness in Drosophila. Neuron *72*, 964–976. https://doi.org/10.1016/j.neuron.2011.12.003.

86. Tanaka, S., Honda, Y., Sawachika, M., Futani, K., Yoshida, N., and Kodama, T. (2022). Degradation of STK16 via KCTD17 with Ubiquitin–Proteasome System in Relation to Sleep–Wake Cycle. Kinases Phosphatases *1*, 14–22. https://doi.org/10.3390/kinasesphosphatases1010003.

87. Naidoo, N., Ferber, M., Master, M., Zhu, Y., and Pack, A.I. (2008). Aging Impairs the Unfolded Protein Response to Sleep Deprivation and Leads to Proapoptotic Signaling. J. Neurosci. *28*, 6539–6548. https://doi.org/10.1523/JNEUROSCI.5685-07.2008.

88. Cunha, C., Brambilla, R., and Thomas, K.L. (2010). A simple role for BDNF in learning and memory? Front. Mol. Neurosci. *3*, 1. https://doi.org/10.3389/neuro.02.001.2010.

89. Miranda, M., Morici, J.F., Zanoni, M.B., and Bekinschtein, P. (2019). Brain-Derived Neurotrophic Factor: A Key Molecule for Memory in the Healthy and the Pathological Brain. Front. Cell. Neurosci. *13*, 363. https://doi.org/10.3389/fncel.2019.00363.

90. Barco, A., Patterson, S., Alarcon, J.M., Gromova, P., Mata-Roig, M., Morozov, A., and Kandel, E.R. (2005). Gene Expression Profiling of Facilitated L-LTP in VP16-CREB Mice Reveals that BDNF Is Critical for the Maintenance of LTP and Its Synaptic Capture. Neuron *48*, 123–137. https://doi.org/10.1016/j.neuron.2005.09.005.

91. Kida, S. (2012). A Functional Role for CREB as a Positive Regulator of Memory Formation and LTP. Exp. Neurobiol. *21*, 136–140. https://doi.org/10.5607/en.2012.21.4.136.

92. Kushikata, T., Fang, J., and Krueger, J.M. (1999). Brain-derived neurotrophic factor enhances spontaneous sleep in rats and rabbits. Am. J. Physiol. *276*, R1334–R1338. https://doi.org/10.1152/ajpregu.1999.276.5.R1334.

93. Takahashi, S., and Krueger, J.M. (1999). Nerve growth factor enhances sleep in rabbits. Neurosci. Lett. *264*, 149–152. https://doi.org/10.1016/s0304-3940(99)00196-2.

94. Kushikata, T., Kubota, T., Fang, J., and Krueger, J.M. (2003). Neurotrophins 3 and 4 enhance non-rapid eye movement sleep in rabbits. Neurosci. Lett. *346*, 161–164. https://doi.org/10.1016/s0304-3940(03)00564-0.

95. Spedding, M., and Gressens, P. (2008). Neurotrophins and cytokines in neuronal plasticity. Novartis Found. Symp. *289*, 222–240. https://doi.org/10.1002/9780470751251.ch18.

96. Mattson, M.P. (2005). Neurotrophic factors and sleep. In Advances in Cell Aging and Gerontology Sleep and Aging (Elsevier), pp. 155–164. https://doi.org/10.1016/S1566-3124(04)17006-5.

97. Gómez-Palacio-Schjetnan, A., and Escobar, M.L. (2013). Neurotrophins and synaptic plasticity. Curr. Top. Behav. Neurosci. *15*, 117–136. https://doi.org/10.1007/7854_2012_231.

98. Krueger, J.M., Nguyen, J.T., Dykstra-Aiello, C.J., and Taishi, P. (2019). Local sleep. Rev. *43*, 14–21. https://doi.org/10.1016/j.smrv.2018.10.001.

99. Huang, E.J., and Reichardt, L.F. (2001). Neurotrophins: Roles in Neuronal Development and Function. Annu. Rev. Neurosci. *24*, 677–736. https://doi.org/10.1146/annurev.neuro.24.1.677.

100. Gonzalez, G.A., Yamamoto, K.K., Fischer, W.H., Karr, D., Menzel, P., Biggs III, W., Vale, W.W., and Montminy, M.R. (1989). A cluster of phosphorylation sites on the cyclic AMP-regulated nuclear factor CREB predicted by its sequence. Nature *337*, 749–752. https://doi.org/10.1038/337749a0.

101. Sheng, M., Thompson, M.A., and Greenberg, M.E. (1991). CREB: a Ca2+-Regulated Transcription Factor Phosphorylated by Calmodulin-Dependent Kinases. Science *252*, 1427–1430. https://www.science.org/doi/10.1126/science.1646483?keytype2=tf_ipsecsha&ijkey=31781d14fb2df05d889694042408407496dac8e2.

102. Bito, H., Deisseroth, K., and Tsien, R.W. (1997). Ca2+-dependent regulation in neuronal gene expression. Curr. Opin. Neurobiol. *7*, 419–429. https://doi.org/10.1016/s0959-4388(97)80072-4.

103. Wong-Riley, M. (1979). Changes in the visual system of monocularly sutured or enucleated cats demonstrable with cytochrome oxidase histochemistry. Brain Res. *171*, 11–28. https://doi.org/10.1016/0006-8993(79)90728-5.

104. Davis, S., Vanhoutte, P., Pagès, C., Caboche, J., and Laroche, S. (2000). The MAPK/ERK Cascade Targets Both Elk-1 and cAMP Response Element-Binding Protein to Control Long-Term Potentiation-Dependent Gene Expression in the Dentate Gyrus In Vivo. J. Neurosci. *20*, 4563–4572. https://doi.org/10.1523/JNEUROSCI.20-12-04563.2000.

105. Ying, S.-W., Futter, M., Rosenblum, K., Webber, M.J., Hunt, S.P., Bliss, T.V.P., and Bramham, C.R. (2002). Brain-Derived Neurotrophic Factor Induces Long-Term Potentiation in Intact Adult Hippocampus: Requirement for ERK Activation Coupled to CREB and Upregulation of Arc Synthesis. J. Neurosci. *22*, 1532–1540. https://doi.org/10.1523/JNEUROSCI.22-05-01532.2002.

106. Silva, A.J., Kogan, J.H., Frankland, P.W., and Kida, S. (1998). CREB and memory. Annu. Rev. Neurosci. *21*, 127–148. https://doi.org/10.1146/annurev.neuro.21.1.127.

107. Glazewski, S., Barth, A.L., Wallace, H., McKenna, M., Silva, A., and Fox, K. (1999). Impaired Experience-dependent Plasticity in Barrel Cortex of Mice Lacking the Alpha and Delta Isoforms of CREB. Cerebr. Cortex *9*, 249–256. https://doi.org/10.1093/cercor/9.3.249.

108. Barth, A.L., McKenna, M., Glazewski, S., Hill, P., Impey, S., Storm, D., and Fox, K. (2000). Upregulation of cAMP Response Element-Mediated Gene Expression during Experience-Dependent Plasticity in Adult Neocortex. J. Neurosci. *20*, 4206–4216. https://doi.org/10.1523/JNEUROSCI.20-11-04206.2000.

109. Wimmer, M.E., Cui, R., Blackwell, J.M., and Abel, T. (2021). Cyclic AMP response element-binding protein is required in excitatory neurons in the forebrain to sustain wakefulness. Sleep *44*, zsaa267. https://doi.org/10.1093/sleep/zsaa267.

110. Bartsch, D., Casadio, A., Karl, K.A., Serodio, P., and Kandel, E.R. (1998). CREB1 encodes a nuclear activator, a repressor, and a cytoplasmic modulator that form a regulatory unit critical for long-term facilitation. Cell *95*, 211–223. https://doi.org/10.1016/s0092-8674(00)81752-3.

111. Upadhya, S.C., Smith, T.K., and Hegde, A.N. (2004). Ubiquitin-proteasome-mediated CREB repressor degradation during induction of long-term facilitation. J. Neurochem. *91*, 210–219. https://doi.org/10.1111/j.1471-4159.2004.02707.x.

112. Buzsáki, G., Anastassiou, C.A., and Koch, C. (2012). The origin of extracellular fields and currents–EEG, ECoG, LFP and spikes. Nat. Rev. Neurosci. *13*, 407–420. https://doi.org/10.1038/nrn3241.

113. Musall, S., von Pföstl, V., Rauch, A., Logothetis, N.K., and Whittingstall, K. (2014). Effects of neural synchrony on surface EEG. Cereb. Cortex N. Y. N *24*, 1045–1053. https://doi.org/10.1093/cercor/bhs389.

114. Rodriguez, A.V., Funk, C.M., Vyazovskiy, V.V., Nir, Y., Tononi, G., and Cirelli, C. (2016). Why Does Sleep Slow-Wave Activity Increase After Extended Wake? Assessing the Effects of Increased Cortical Firing During Wake and Sleep. J. Neurosci. *36*, 12436–12447. https://doi.org/10.1523/JNEUROSCI.1614-16.2016.

115. Hubbard, J., Gent, T.C., Hoekstra, M.M.B., Emmenegger, Y., Mongrain, V., Landolt, H.-P., Adamantidis, A.R., and Franken, P. (2020). Rapid fast-delta decay following prolonged wakefulness marks a phase of wake-inertia in NREM sleep. Nat. Commun. *11*, 3130. https://doi.org/10.1038/s41467-020-16915-0.

116. Lewis, L.D., Voigts, J., Flores, F.J., Schmitt, L.I., Wilson, M.A., Halassa, M.M., and Brown, E.N. (2015). Thalamic reticular nucleus induces fast and local modulation of arousal state. Elife *4*, e08760. https://doi.org/10.7554/eLife.08760.

117. Amzica, F., and Steriade, M. (1998). Electrophysiological correlates of sleep delta waves. Clin. Neurophysiol. *107*, 69–83. https://doi.org/10.1016/S0013-4694(98)00051-0.

118. Hofer, M., Pagliusi, S.R., Hohn, A., Leibrock, J., and Barde, Y.A. (1990). Regional distribution of brain-derived neurotrophic factor mRNA in the adult mouse brain. EMBO J. *9*, 2459–2464. https://doi.org/10.1002/j.1460-2075.1990.tb07423.x.

119. Rocamora, N., Welker, E., Pascual, M., and Soriano, E. (1996). Upregulation of BDNF mRNA Expression in the Barrel Cortex of Adult Mice after Sensory Stimulation. J. Neurosci. *16*, 4411–4419. https://doi.org/10.1523/JNEUROSCI.16-14-04411.1996.

120. Croll, S.D., Wiegand, S.J., Anderson, K.D., Lindsay, R.M., and Nawa, H. (1994). Regulation of neuropeptides in adult rat forebrain by the neurotrophins BDNF and NGF. Eur. J. Neurosci. *6*, 1343–1353. https://doi.org/10.1111/j.1460-9568.1994.tb00325.x.

121. Nawa, H., Pelleymounter, M.A., and Carnahan, J. (1994). Intraventricular administration of BDNF increases neuropeptide expression in newborn rat brain. J. Neurosci. *14*, 3751–3765. https://doi.org/10.1523/JNEUROSCI.14-06-03751.1994.

122. Conner, J.M., Lauterborn, J.C., Yan, Q., Gall, C.M., and Varon, S. (1997). Distribution of Brain-Derived Neurotrophic Factor (BDNF) Protein and mRNA in the Normal Adult Rat CNS: Evidence for Anterograde Axonal Transport. J. Neurosci. *17*, 2295–2313. https://doi.org/10.1523/JNEUROSCI.17-07-02295.1997.

123. Andreska, T., Rauskolb, S., Schukraft, N., Lüningschrör, P., Sasi, M., Signoret-Genest, J., Behringer, M., Blum, R., Sauer, M., Tovote, P., and Sendtner, M. (2020). Induction of BDNF Expression in Layer II/III and Layer V Neurons of the Motor Cortex Is Essential for Motor Learning. J. Neurosci. *40*, 6289–6308. https://doi.org/10.1523/JNEUROSCI.0288-20.2020.

124. Cabelli, R.J., Allendoerfer, K.L., Radeke, M.J., Welcher, A.A., Feinstein, S.C., and Shatz, C.J. (1996). Changing Patterns of Expression and Subcellular Localization of TrkB in the Developing Visual System. J. Neurosci. *16*, 7965–7980. https://doi.org/10.1523/JNEUROSCI.16-24-07965.1996.

125. Cellerino, A., Maffei, L., and Domenici, L. (1996). The distribution of brain-derived neurotrophic factor and its receptor trkB in parvalbumin-containing neurons of the rat visual cortex. Eur. J. Neurosci. *8*, 1190–1197. https://doi.org/10.1111/j.1460-9568.1996.tb01287.x.

126. Chauvette, S., Volgushev, M., and Timofeev, I. (2010). Origin of Active States in Local Neocortical Networks during Slow Sleep Oscillation. Cerebr. Cortex *20*, 2660–2674. https://doi.org/10.1093/cercor/bhq009.

127. Krone, L.B., Yamagata, T., Blanco-Duque, C., Guillaumin, M.C.C., Kahn, M.C., van der Vinne, V., McKillop, L.E., Tam, S.K.E., Peirson, S.N., Akerman, C.J., et al. (2021). A role for the cortex in sleep-wake regulation. Nat. Neurosci. *24*, 1210–1215. https://doi.org/10.1038/s41593-021-00894-6.

128. Gottschalk, W., Pozzo-Miller, L.D., Figurov, A., and Lu, B. (1998). Presynaptic Modulation of Synaptic Transmission and Plasticity by Brain-Derived Neurotrophic Factor in the Developing Hippocampus. J. Neurosci. *18*, 6830–6839. https://doi.org/10.1523/JNEUROSCI.18-17-06830.1998.

129. Figurov, A., Pozzo-Miller, L.D., Olafsson, P., Wang, T., and Lu, B. (1996). Regulation of synaptic responses to high-frequency stimulation and LTP by neurotrophins in the hippocampus. Nature *381*, 706–709. https://doi.org/10.1038/381706a0.

130. Lu, Y., Christian, K., and Lu, B. (2008). BDNF: A Key Regulator for Protein-synthesis Dependent LTP and Long-term Memory? Neurobiol. Learn. Mem. *89*, 312–323. https://doi.org/10.1016/j.nlm.2007.08.018.

131. Leal, G., Comprido, D., and Duarte, C.B. (2014). BDNF-induced local protein synthesis and synaptic plasticity. Neuropharmacology *76 Pt C*, 639–656. https://doi.org/10.1016/j.neuropharm.2013.04.005.

132. Solinas, S.M.G., Edelmann, E., Leßmann, V., and Migliore, M. (2019). A kinetic model for Brain-Derived Neurotrophic Factor mediated spike timing-dependent LTP. PLoS Comput. Biol. *15*, e1006975. https://doi.org/10.1371/journal.pcbi.1006975.

133. Toyoizumi, T., Kaneko, M., Stryker, M.P., and Miller, K.D. (2014). Modeling the dynamic interaction of Hebbian and homeostatic plasticity. Neuron *84*, 497–510. https://doi.org/10.1016/j.neuron.2014.09.036.

134. D'Ambrosio, S., Castelnovo, A., Guglielmi, O., Nobili, L., Sarasso, S., and Garbarino, S. (2019). Sleepiness as a Local Phenomenon. Front. Neurosci. *13*, 1086. https://doi.org/10.3389/fnins.2019.01086.

135. Andrillon, T., Windt, J., Silk, T., Drummond, S.P.A., Bellgrove, M.A., and Tsuchiya, N. (2019). Does the Mind Wander When the Brain Takes a Break? Local Sleep in Wakefulness, Attentional Lapses and Mind-Wandering. Front. Neurosci. *13*, 949. https://doi.org/10.3389/fnins.2019.00949.

136. Schindelin, J., Arganda-Carreras, I., Frise, E., Kaynig, V., Longair, M., Pietzsch, T., Preibisch, S., Rueden, C., Saalfeld, S., Schmid, B., et al. (2012). Fiji: an open-source platform for biological-image analysis. Nat. Methods *9*, 676–682. https://doi.org/10.1038/nmeth.2019.

137. Miladinović, Đ., Muheim, C., Bauer, S., Spinnler, A., Noain, D., Bandarabadi, M., Gallusser, B., Krummenacher, G., Baumann, C., Adamantidis, A., et al. (2019). SPINDLE: End-to-end learning from EEG/EMG to extrapolate animal sleep scoring across experimental settings, labs and species. PLoS Comput. Biol. *15*, e1006968. https://doi.org/10.1371/journal.pcbi.1006968.

138. Tyanova, S., Temu, T., Sinitcyn, P., Carlson, A., Hein, M.Y., Geiger, T., Mann, M., and Cox, J. (2016). The Perseus computational platform for comprehensive analysis of (prote)omics data. Nat. Methods *13*, 731–740. https://doi.org/10.1038/nmeth.3901.

139. Evangelista, J.E., Xie, Z., Marino, G.B., Nguyen, N., Clarke, D.J.B., and Ma'ayan, A. (2023). Enrichr-KG: bridging enrichment analysis across multiple libraries. Nucleic Acids Res. *51*, W168–W179. https://doi.org/10.1093/nar/gkad393.

140. Ge, S.X., Jung, D., and Yao, R. (2020). ShinyGO: a graphical gene-set enrichment tool for animals and plants. Bioinformatics *36*, 2628–2629. https://doi.org/10.1093/bioinformatics/btz931.

141. Szklarczyk, D., Gable, A.L., Lyon, D., Junge, A., Wyder, S., Huerta-Cepas, J., Simonovic, M., Doncheva, N.T., Morris, J.H., Bork, P., et al. (2019). STRING v11: protein-protein association networks with increased coverage, supporting functional discovery in genome-wide experimental datasets. Nucleic Acids Res. *47*, D607–D613. https://doi.org/10.1093/nar/gky1131.

142. Tobler, I., and Jaggi, K. (1987). Sleep and EEG spectra in the Syrian hamster (Mesocricetus auratus) under baseline conditions and following sleep deprivation. J. Comp. Physiol. *161*, 449–459. https://doi.org/10.1007/BF00603970.

143. Curie, T., Mongrain, V., Dorsaz, S., Mang, G.M., Emmenegger, Y., and Franken, P. (2013). Homeostatic and Circadian Contribution to EEG and Molecular State Variables of Sleep Regulation. Sleep *36*, 311–323. https://doi.org/10.5665/sleep.2440.

144. Gent, T.C., Bandarabadi, M., Herrera, C.G., and Adamantidis, A.R. (2018). Thalamic dual control of sleep and wakefulness. Nat. Neurosci. *21*, 974–984. https://doi.org/10.1038/s41593-018-0164-7.

145. Franken, P., Dijk, D.-J., Tobler, I., and Borbély, A.A. (1994). High-frequency components of the rat electrocorticogram are modulated by the vigilance states. Neurosci. Lett. *167*, 89–92. https://doi.org/10.1016/0304-3940(94)91034-0.

146. Fattinger, S., Jenni, O.G., Schmitt, B., Achermann, P., and Huber, R. (2014). Overnight Changes in the Slope of Sleep Slow Waves during Infancy. Sleep *37*, 245–253. https://doi.org/10.5665/sleep.3390.

147. Quiroga, R.Q., Nadasdy, Z., and Ben-Shaul, Y. (2004). Unsupervised Spike Detection and Sorting with Wavelets and Superparamagnetic Clustering. Neural Comput. *16*, 1661–1687. https://doi.org/10.1162/089976604774201631.

148. Chaure, F.J., Rey, H.G., and Quian Quiroga, R. (2018). A novel and fully automatic spike-sorting implementation with variable number of features. J. Neurophysiol. *120*, 1859–1871. https://doi.org/10.1152/jn.00339.2018.

149. Kuleshov, M.V., Jones, M.R., Rouillard, A.D., Fernandez, N.F., Duan, Q., Wang, Z., Koplev, S., Jenkins, S.L., Jagodnik, K.M., Lachmann, A., et al. (2016). Enrichr: a comprehensive gene set enrichment analysis web server 2016 update. Nucleic Acids Res. *44*, W90–W97. https://doi.org/10.1093/nar/gkw377.

150. Chen, E.Y., Tan, C.M., Kou, Y., Duan, Q., Wang, Z., Meirelles, G.V., Clark, N.R., and Ma'ayan, A. (2013). Enrichr: interactive and collaborative HTML5 gene list enrichment analysis tool. BMC Bioinf. *14*, 128. https://doi.org/10.1186/1471-2105-14-128.

151. Snel, B., Lehmann, G., Bork, P., and Huynen, M.A. (2000). STRING: a web-server to retrieve and display the repeatedly occurring neighbourhood of a gene. Nucleic Acids Res. *28*, 3442–3444. https://doi.org/10.1093/nar/28.18.3442.

152. Van Dongen, S. (2008). Graph Clustering Via a Discrete Uncoupling Process. SIAM J. Matrix Anal. Appl. *30*, 121–141. https://doi.org/10.1137/040608635.

153. Liu, Z.-P., Wu, C., Miao, H., and Wu, H. (2015). RegNetwork: an integrated database of transcriptional and post-transcriptional regulatory networks in human and mouse. Database *2015*, bav095. https://doi.org/10.1093/database/bav095.

154. Brüning, F., Noya, S.B., Bange, T., Koutsouli, S., Rudolph, J.D., Tyagarajan, S.K., Cox, J., Mann, M., Brown, S.A., and Robles, M.S. (2019). Sleep-wake cycles drive daily dynamics of synaptic phosphorylation. Science *366*, eaav3617. https://doi.org/10.1126/science.aav3617.

155. Humphrey, S.J., Karayel, O., James, D.E., and Mann, M. (2018). High-throughput and high-sensitivity phosphoproteomics with the EasyPhos platform. Nat. Protoc. *13*, 1897–1916.

156. Demichev, V., Messner, C.B., Vernardis, S.I., Lilley, K.S., and Ralser, M. (2020). DIA-NN: neural networks and interference correction enable deep proteome coverage in high throughput. Nat. Methods *17*, 41–44. https://doi.org/10.1038/s41592-019-0638-x.

157. Bazhenov, M., Timofeev, I., Steriade, M., and Sejnowski, T.J. (2002). Model of thalamocortical slow-wave sleep oscillations and transitions to activated States. J. Neurosci. *22*, 8691–8704. https://doi.org/10.1523/JNEUROSCI.22-19-08691.2002.

158. Compte, A., Sanchez-Vives, M.V., McCormick, D.A., and Wang, X.-J. (2003). Cellular and network mechanisms of slow oscillatory activity (<1 Hz) and wave propagations in a cortical network model. J. Neurophysiol. *89*, 2707–2725. https://doi.org/10.1152/jn.00845.2002.

159. Hill, S., and Tononi, G. (2005). Modeling sleep and wakefulness in the thalamocortical system. J. Neurophysiol. *93*, 1671–1698. https://doi.org/10.1152/jn.00915.2004.

160. Tatsuki, F., Sunagawa, G.A., Shi, S., Susaki, E.A., Yukinaga, H., Perrin, D., Sumiyama, K., Ukai-Tadenuma, M., Fujishima, H., Ohno, R., et al. (2016). Involvement of Ca(2+)-Dependent Hyperpolarization in Sleep Duration in Mammals. Neuron *90*, 70–85. https://doi.org/10.1016/j.neuron.2016.02.032.

STAR★METHODS

KEY RESOURCES TABLE

REAGENT or RESOURCE	SOURCE	IDENTIFIER
Antibodies		
Chicken polyclonal anti-mCherry (1:2000)	Abcam	Cat# ab205402
Guineapig polyclonal anti-NeuN (1:1000)	Synaptic Systems	Cat# 266 004
Rabbit monoclonal anti-HA-tag (1:1000)	Cell Signaling Technologies	Cat# 3724
Goat Anti-Chicken Cy3 preabsorbed (1:500)	Abcam	Cat# ab97145
Goat Anti-Guinea Pig Alexa Fluor 647 (1:2000)	Jackson	Cat# 106-605-003
Goat Anti-rabbit Alexa Fluor 488 (1:1000)	Invitrogen	Cat# A11008, Lot: 1622775
Chicken anti-GFP (1:500)	Aves lab	Cat# GFP-1010, Lot 3717982
Goat anti-chicken IgY H&L A488 (1:1000)	Abcam	Cat# ab150169
Bacterial and virus strains		
ssAAV-5/2-hSyn1-hM3D(Gq)-mCherry-WPRE-hGHp(A) (5.0 x 10E12 vg/mL)	VVF (ordered from Addgene #50474)	v101-5
ssAAV-5/2-hSyn1-mCherry-WPRE-hGHp(A) (5.0 x 10E12 vg/mL)	VVF (modified from Addgene #50474)	v253-5
ssAAV-5/2-mCaMKIIα-hChR2(H134R)-mCherry-WPRE-hGHp(A) (5.0 x 10E12 vg/mL)	VVF (ordered from Addgene #26975)	v204-5
ssAAV-5/2-mCaMKIIa(short)-OptoB(E281A)-HA-WPRE-hGHp(A) (5.0 x 10E12 vg/mL)	VVF (provided by Hong and Heo[51])	vSB3-5
ssAAV-5/2-hSyn1-dlox-OptoB(E281A)-HA(rev)-dlox-WPRE-hGHp(A) (5.0 x 10E12 vg/mL)	VVF (provided by Hong and Heo[51])	vSB4-5
ssAAV-5/2-hSyn1-dlox-HA_rM3D(Gs)_IRES_mCitrine(rev)-dlox-WPRE-hGHp(A) (7.4 x 10E12 vg/mL)	VVF (ordered from Addgene #50456)	v111-5
Chemicals, peptides, and recombinant proteins		
666–15	TOCRIS	Cat# 5661, batch No.2
BDNF	R & D Systems	Cat# 248-BDB-250/CF
K252a	alomone labs	Cat# 97161-97-2
Actinomycin D	Sigma	Cat# A9415-2MG
Trimethoprim	Selleckchem	Cat# S3129
Anisomycin	Raybiotech	Cat# 331-21892-2
Critical commercial assays		
RNA purification Micro-Kit	NORGEN CORP	Cat# 35300,35350
Agilent RNA ScreenTape Quick	Agilent Technologies Inc.	Cat# Agilent 4200
Deposited data		
EEG data	This paper	Zenodo: https://doi.org/10.5281/zenodo.8377990
Modeling data	This paper	Zenodo: https://doi.org/10.5281/zenodo.10206425
RNA-seq data	This paper	ENA: PRJEB66436
mass spectrometry proteomics data	This paper	ProteomeXchange: PXD045652
Experimental models: Organisms/strains		
RasGRF2a-dCre (L2-3): B6; 129S-Rasgrf2<tm1.1(Cre/folA)Hze>/J	The Jackson Laboratory	Cat# 24727
Rbp-4Cre (L5): STOCK Tg(Rbp4 Cre) KL100Gsat/Mmucd	MMRRC	Cat# 31125
Ntsr1-Cre (L6): STOCK Tg(Ntsr1-Cre) GN220Gsat/Mmucd	MMRRC	Cat# 30648

Continued

REAGENT or RESOURCE	SOURCE	IDENTIFIER
VGAT-Cre: B6J.129S6(FVB)-Slc32a1<tm2(Cre)Lowl>/MwarJ	The Jackson Laboratory	Cat# 028862
Software and algorithms		
ImageJ/FiJI	NIH Schindelin et al.[136]	https://imagej.net/software/fiji/
MATLAB	MathWorks R2020b	https://www.mathworks.com/products/matlab.html
RHD data acquisition software	Intan Technologies	RHD2000
Signal Express NI 2015	National Instruments	https://www.ni.com/en/support/downloads/software-products/download.signalexpress.html#322415
LABVIEW	National Instruments	https://www.ni.com/en/support/downloads/software-products/download.labview.html#521715
SPINDLE	Miladinović et al.[137]	https://sleeplearning.ethz.ch/
R	The R Project for Statistical Computing	https://www.r-project.org/
Perseus	Tyanova et al.[138]	https://maxquant.net/perseus/
Multi-Channel Experimenter software	Multi Channel Systems	https://www.multichannelsystems.com/downloads
Enrichr-KG	Evangelista et al.[139]	https://maayanlab.cloud/enrichr-kg
ShinyGO 0.77	Ge et al.[140]	http://bioinformatics.sdstate.edu/go77/
STRING (v11.5)	Szklarczyk et al.[141]	https://string-db.org/
GraphPad Prism 9	Graphpad	https://www.graphpad.com/features
Biorender	Biorender	https://app.biorender.com/
Morpheus	Morpheus	https://software.broadinstitute.org/morpheus
Inkscape	Inkscape	https://inkscape.org/
Other		
optorodes	Thorlabs,Inc	Cat# CFLC440-10; Cat# FT400UMT
4-channel LED driver	Thorlabs,Inc	Cat# DC4104
4-channels hub	Thorlabs,Inc	Cat# DC4100-HUB
LED light source	Thorlabs,Inc	Cat# M470F3,470 nm
patch cable	Thorlabs,Inc	Cat# FT400EMT-custom
ceramic mating sleeve	Thorlabs,Inc	Cat# ADAL1-5
power meter	Thorlabs,Inc	Cat# PM100A
electrode interface board	NeuraLynx	Cat# EIB-36
sliding microtome	Histocom AG	Cat# HYRAX S 50
headstage amplifier chip	Intan Technologies	Cat# RHD2132
Cannula	Plastics One Inc.	Cat# C315IA

RESOURCE AVAILABILITY

Lead contact

Further information and requests for resources and reagents should be directed to and will be fulfilled upon request by the lead contact, Waleed ElGrawani (wal33d91@gmail.com).

Materials availability

No new materials have been generated in this manuscript.

Data and code availability

- The mass spectrometry proteomics data have been deposited to the ProteomeXchange Consortium via the PRIDE partner repository with the dataset identifier "ProteomeXchange: PXD045652." Transcriptomics data have been deposited in the

European Nucleotide Archive (ENA) at EMBL-EBI under accession numbers "ENA: PRJEB66436." EEG and modeling data have been deposited to https://doi.org/10.5281/zenodo.8377990 and https://doi.org/10.5281/zenodo.10206425.
- This paper does not report original code.
- Any additional information required to reanalyze the data reported in this work paper is available from the lead contact upon request.

EXPERIMENTAL MODEL AND STUDY PARTICIPANT DETAILS

Animals

All experiments were performed with the approval of animal welfare officers at the University of Zurich and relevant veterinary authorities of cantons Zurich and Bern in Switzerland. Experiments were performed in male mice with age range between (10–15 weeks). Mice were housed in T3 open-top transparent type cages with *ad libitum* food and water under 12h light:12h dark cycles. All experiments (except for Cre-expressing strains in Figures 2; S3, S4, and S8; see key resources table) were performed on C57BL/6JRj species purchased from Janvier Labs. Mice were housed in groups of 2–4 mice per cage with proper environmental enrichment but were individually housed after implantation surgeries for electrophysiological recordings or optogenetics. Sleep deprivations were performed using gentle handling and continuous introduction of novel objects into cages.[142]

METHOD DETAILS

Surgeries

Mice received an appropriate dose of Temgesic analgesia (0.1 mg/kg, intraperitoneal) at least 30 min before mounting on a stereotactic frame for surgery. All surgeries were performed under isoflurane anesthesia (1.5–2%). Additionally, lidocaine (10 mg/mL, subcutaneous) was locally applied before the start of surgery.

AAV injections

Mice were injected using a custom-made glass pipette attached to a 701 RN 10 μL Hamilton syringe. A volume of 1.5 μL was injected at the rate of 120 nL per minute into the coordinates (bregma: −1.6 ML, −1.8 AP). To target L2/3 and L4, the needle was respectively inserted −0.35 mm and −0.5 mm below the cortical surface. For all other experiments, the needle was inserted −0.75 mm inside the cortex. To prevent suction of any liquid particles, the needle was gradually withdrawn 10 min after the injection was completed. All Adeno-associated viruses (AAVs) were prepared in a solvent of 1x PBS, pH 7.4, 1 mM MgCl2, 2.5 mM KCl. All AAVs were produced by the Viral Vector Facility (VVF) at the University of Zurich. A list of AAVs along with their corresponding physical titer is provided in key resources table. After the surgeries, the mice were transferred back to sterile home cages and housed in groups while being continuously monitored during their recovery period. For mice that were utilized for immunostaining or acute brain slice preparations, a minimum of 3 weeks were given before conducting experiments to ensure adequate AAV expression. For EEG recordings and optogenetics experiments, mice were subjected to a second surgery of implantations ≈12–14 days following the intracranial AAV injection. For RasGRF2a-dCre mice, to prevent proteasomal degradation of dCre, they received intraperitoneal injections of Trimethoprim (Selleckchem, #S3129, 150 μg per g of mouse body weight) twice: 14 and 16 days following AAV delivery. Trimethoprim was prepared as a stock solution of 100 mg/mL in DMSO, sonicated for 15 min, filtered, and freshly diluted in vehicle (20% PEG-400 in saline) before intraperitoneal injection (i.p).

EEG implantations

5 gold-plated EEG screws (0.9 mm) were fixed in the following coordinates: 1 screw in the right parietal (top of injection site), 1 screw in the contralateral left parietal (1.6, −1.8 from bregma), 1 screw in the right frontal (−1.5, 1.2 from bregma), 1 screw in left frontal (1.5,1.2 from bregma), and a screw above the cerebellum (0, −2 from lambda) as a reference. Two golden wires (0.2 mm) were bilaterally inserted in the neck muscle for EMG recording. The 2 frontal screws were typically used for fixation purposes except for Figure S6 where we recorded frontal EEG as a proof of concept of the locality of our assay. Electrodes and EMG wires were connected to stainless steel wires (0.07 mm thickness) soldered to a fine cable. The implants were fixed using dental cement (Paladur 2-component system and TetricEvoFlow). After the implantation procedure, the mice were placed in insulated EEG boxes and connected to a counterbalance and a rotor setup to allow for free movement. A recovery period of at least six days was provided before any recordings started.

Cannula-LFP implantations

Customized pedestal cannulas (Plastics One Inc., C315GA/Spc, cut 0.6 mm below pedestal) were attached to LFP wire (0.127 mm) that protruded 0.2 mm below cannula tip to allow for local recordings from the manipulated network. Cannulas/LFP wire were unihemispherically fixed on top of the injection site (−1.6 ML, −1.8 AP from bregma) in the somatosensory cortex, and the LFP wire was connected to the EEG cable. Contralateral EEG, reference, and EMG were performed as described above. To prevent clogging, a dummy cap with the same acute guide length was always applied and cannulas were controlled for clogging every 2 days.

Optrode-LFP implantations

400 μm optrodes (Thorlabs,Inc, #CFLC440-10, #FT400UMT) were prepared following the general guidelines provided by Thorlabs, and were quality controlled for integrity of light transmission before use. LFP wire was attached to optrodes with projection of 0.2 mm

below the optrode tip. Optrodes were unihemispherically positioned on the injection site (−1.6 ML, −1.8 AP from bregma, and −0.1 to −0.35 DV from cortex surface). Mice were habituated for optical cables for at least 6 days prior to start of experiments.

LFP implantations for whiskers-cut experiment

LFP wire was positioned in right hemisphere barrel cortex (−3 ML, −1.2 AP, −0.75 DV). A contralateral LFP wire inserted in left hemisphere (3 ML, −1.2 AP, −0.75 DV). Reference and EMG were obtained as described above. In experiment day, the right-side whiskers were cut with a fine scissors under less than 3 min of isoflurane anesthesia (1.5–2%). Similarly, the intact whisker group mice were also put in 3 min of isoflurane anesthesia to avoid variations. After whiskers were cut $\approx$ ZT 12, mice were sleep-restricted for 4 h by gentle handling and continuous introduction of novel objects to motivate exploration behavior. In general, mice were quite active at the start of the dark phase. They were checked once every 15 min under low-intensity near-infrared light (<0.5 lux), briefly activated for a few seconds. If found asleep, they were gently awakened to maximize whisker usage during exploration. On average, these mice only spent 4.2 ± 1.3 min asleep within those 4 h of sleep restriction. Since mice have low sleep-drive at the beginning of dark phase, their sleep onset latency following 6 h sleep deprivation is around 2.5 h.[143] Thus, we provided a second injection of k252-a or vehicle at ZT 15 to ensure TrkB signaling is blocked during periods of activity.

Tetrodes-implantations

In general, methods used here mirror those in Gent et al. (2018).[144] Tetrodes were prepared using (California Fine Wire Co., Tungsten,0.0127 mm), gold plated and controlled for conductance before use. Each tetrode was housed in thin FS tubing. 2 tetrodes were glued to the optical fiber so that the tetrodes tips were positioned $\approx$ 0.2mm under the optical fiber, and they were targeted approximately on top of layer 5 of the somatosensory cortex of the right hemisphere (−1.6 ML, −1.8 AP from bregma, and $\approx$ −0.5 to −0.6 DV inside cortex). The other 2 tetrodes were positioned similarly in the contralateral hemisphere. 2 gold-plated screws were positioned frontally (−1.5, 1.2 and 1.5, 1.2 from bregma) to obtain surface EEG signals. Reference and EMG were performed as described above. Tetrodes and other electrodes were collected in an electrode interface board (EIB-36, NeuraLynx). Mice were allowed to recover and habituate for at least 6 days before the experiment.

Immunofluorescence staining

Mice were anesthetized with pentobarbital (0.1 mL, 50 mg/mL solution), and then intracardially perfused with ice-cold 4% paraformaldehyde (PFA) in 0.15 M sodium phosphate buffer (pH 7.4). The brains were extracted, fixed in 4% PFA for 90 min, and cryoprotected in 30% sucrose in PBS at 4°C until they had sunk in the bottom of the solution. Using a sliding microtome (Histocom AG, HYRAX S 50), brains were coronally sectioned into 40 μm slices and stored in an anti-freezing solution (15% glucose, 30% ethylene glycol, 0.02% sodium azide in 50 mM phosphate buffer, pH 7.4) at −20°C. Slices were washed 3 times (10 min each) in Tris-Triton 0.05% (0.05% Triton X-100 in 1x Tris-saline(50 mM Tris, 150 mM NaCl), pH 7.4) at room temperature with agitation at 80 rpm. Brain slices were then incubated overnight in a solution containing primary antibodies, 2% normal serum (from species in which the secondary antibodies were raised), and 0.2% Triton X-100 in 1x Tris-saline. The slices were then washed 3 times, then incubated in a solution containing secondary antibodies, 2% normal serum, and Tris-Triton 0.05% for 30 min at room temperature, followed by a DAPI staining step (Sigma,1μg/mL DAPI in Tris-Triton 0.05%) for 5 min at room temperature. The slices were washed twice in Tris-Triton 0.05% before being mounted onto gelatin-coated glass slides. The slides were then incubated to dry in a dark room, sealed with medium (Dako Ltd., Denmark), covered with cover slips, and stored at 4°C until use. The images were acquired using a confocal laser scanning microscope (Zeiss LSM800), and colocalization was analyzed using built-in function "coloc2" in ImageJ.

Acute slice preparation and ex-vivo multi-electrode recordings

Mice were stereotactically injected with *hSyn1-hM3D(Gq)-mCherry* or *hSyn1-mCherry* (control) adeno-associated virus 5 (AAV5) into the somatosensory cortex. Upon sufficient expression (i.e., $\geq$3 weeks later), mice were sacrificed, and brains were sliced with vibratome in ice-cold artificial cerebro-spinal fluid (ACSF in mM: NaCl, 95; KCl,1.8; KH_2PO_4,1.2; $CaCl_2$,0.5; $MgSO_4$,7; $NaHCO_3$,26; glucose,15; sucrose,50; oxygenated with 95% O_2; 5% CO_2; pH 7.4, measured osmolarity 310 mosmol kg-1). In brief, slices were incubated for at least 1 h in ACSF at room temperature and then transferred to the recording chamber, perfused continuously with oxygenated-ACSF at room temperature. Slices were then placed on top of a 60pMEA100/30iR-Ti-gr perforated array (Multi Channel Systems) and positioned so that electrodes region of the array is in middle of cortical injection site. To ensure proper contact between slice and array, a weight was used in conjugation with suction from underneath. Slices were incubated for at least 30 min in recording chamber before start of recordings and Oxygenated ACSF at 34°C ran continuously through the MEA chamber for the duration of the experiment (1.2 mL/min inflow/17 mL/min outflow + gravity flow inflow/suction outflow at 65). We recorded a baseline and then CNO (10 μM in ACSF) was infused at the same flow rate mentioned above. Slice were exposed to CNO for $\approx$20 min and then we recorded under CNO infusion. Then, CNO infusion was stopped and ACSF (without-CNO) was re-infused for $\approx$20 min before we started a washout recording. Recordings were sampled at 20000 Hz using Multi-Channel Experimenter software (Multi Channel Systems). Data were analyzed using Offline Sorter (Plexon) as follows: signals were run through a Butterworth high pass filter at 300Hz and 'spikes' were detected using a threshold of ±4 Standard Deviations. For each spike the waveform was analyzed, and a unit assigned to each unique waveform detected from an individual electrode using the Valley Seeking spike sorting approach. For firing rate analysis, only stable units firing at a rate $\geq$0.1 Hz (spike count/length of recording file in seconds) were considered. The number of firing units was quantified as the count of units firing $\geq$0.1 Hz per recording file.

***In vivo* recordings in freely behaving mice & analysis**
EEG(LFP)

Recordings always started at light onset (ZT 0). We always started by recording a baseline day where mice were untouched before commencing with the relevant manipulations. Signal acquisition parameters were set using Signal Express NI 2015 controlled via LABVIEW. The signals were amplified with amplification factor of ≈2000, analog band-pass filtered (high pass filter: −3 dB at 0.016 Hz; low pass filter: −3 dB at 40 Hz), sampled at 10240 Hz, then decimated and stored with 512 Hz resolution in European Data Format (EDF) file. For cannula-EEG experiments: a different EEG setup was used with the same parameters but with a sampling rate of 1024 Hz, then signals were decimated and stored with 128 Hz resolution in EDF file. The EEG and EMG signals were digitally band-pass filtered using MATLAB function "cheby2" (between 0.1 and 40 Hz for EEG and 10 to 30 Hz for EMG), downsampled, and stored with a final resolution of 128 Hz. The power spectral density was computed for 4-s epochs using MATLAB "pwelch" estimate (0.25 Hz resolution bins with no overlap hanning window). Adjacent 0.25 Hz bins were averaged and stored as 0.5 Hz bins for frequencies between 0.5 and 5 Hz and 1 Hz bins for frequencies between 5.25 and 25 Hz. Before each recording, the EEG and EMG channels were calibrated with a 10 Hz, 300 μV peak-to-peak sine wave. Vigilance states (NREM, REM and wake) were automatically detected using SPINDLE machine learning server[137] and raw traces were visually inspected, according to criteria described in Franken et al. (1994),[145] for validation. Epochs with artifacts on either LFP or EEG signals were simultaneously excluded from power spectral analysis in all derivations. Mice were excluded from the analysis if raw traces of either LFP or EEG signals were dominated by artifacts. To ensure robust interhemispheric comparison, mice with poor signal quality, such as low amplitude signal that is indistinguishable from the noise level, in either brain hemisphere were excluded from the study. Slow wave activity (SWA) was calculated, in 1-h intervals, as average of NREM spectral power density bins between 0.75 and 4 Hz (unless stated otherwise) and normalized to the average of delta power (0.75–4 Hz) of 12 h (ZT 0–12) of the same vigilance state in baseline day (unless stated otherwise). Power spectra plots represent the power density between (0.75–25 Hz) binned as following: low delta (δ1: 0.75–2 Hz), high delta (δ2: 2.25–4 Hz), theta (θ:5–8 Hz), alpha (α:9–12 Hz), and beta (β: 13–25 Hz). The power spectrum was normalized as follows: power in each frequency band was normalized to the 12-h power average of the same frequency band in the same vigilance state in baseline day (ZT 0–12). Note that frequencies technically affected by the 10 Hz optogenetic stimulation of ChR2 (i.e., 10, 11, 20, 21 Hz; Figure S7) were excluded from the power spectrum analysis. All the analysis was done via custom-made scripts in MATLAB (MathWorks R2020b).

Detection of individual sleep slow waves was performed using automated detection algorithm using similar approach as reported by Fattinger et al. (2014).[146] EEG signals were band-pass filtered (MATLAB "cheby2", passband 1 and 4.0 Hz, stop-band: <0.1 and >8 Hz) using a zero-phase digital filtering (MATLAB "filtfilt"). Automated detection of slow waves during artifact-free NREM-sleep epochs was performed based on negative zero crossing approach (i.e., negative deflection of the EEG signals between 2 consecutive zero-crossings). Local minima of the negative deflections were considered as negative peak amplitude, and descending and ascending slopes were calculated based timestamps of zero crossings and negative peaks as following:

$$descending\ slope = \frac{neg.peak\ amplitude}{t1 - t2}\ \ ascending\ slope = \frac{neg.peak\ amplitude}{t3 - t2}$$

where t1 is the timestamp of the negative peak, t2 is timestamp of the previous zero-crossing, and t3 is timestamp for following zero crossing.

The maximum positive point following the corresponding negative peak were detected and peak to peak (i.e., peak to trough) amplitude was calculated. Positive peak amplitude was calculated as difference between peak-to-peak and negative-peak amplitude. Amplitudes of negative and positive peaks and slopes were calculated after stimulation (ZT 9-12) and represented as a relative change to before stimulation (ZT 0-6) in Figure 2D.

***Invivo* multi-electrode array recording**

Mice were habituated to headstage amplifier chip (RHD2132, Intan Technologies) and cables for at least 1 h daily for 6 days prior to experiment. Signals were acquired at sample rate of 20000 Hz using free open-source software (RHD2000, Intan Technologies). We recorded 1 h at ZT 2 and 1 h at ZT 7 on baseline day. For stimulation day, we recorded the same hours and stimulation (1s per 5s for 2 h) was performed between ZT 2 and ZT 4. We selected ZT 2 as a control prior to stimulation, while ZT 7 was chosen as a time window of high local upregulation of SWA in response to TrkB stimulation, based on previous experiments with LFP recordings. EEG/EMG signals were decimated (MATLAB "decimate") and stored with 250 Hz resolution, then used for scoring vigilance states as described above.

In parallel, unit activity of the different tetrode channels were analyzed on original data files (20000 Hz sampled) using MATLAB "wave_clus" package originally published in Quiroga et al. (2004)[147] and adapted by Chaure et al. (2018).[148] The raw traces recorded at ZT 2 and ZT 7 were concatenated together as a single trace for each channel and spikes detection (MATLAB "Get_spikes") and sorting (MATLAB "Do_clustering") were performed on the concatenated traces to avoid mismatching of units detected between the 2 time points. This algorithm uses wavelet decomposition to extract features of spike waveforms and superparamagnetic clustering (SPC) to cluster the spikes in this feature space. Clusters were visually validated by visual inspection of inter-spike interval (isi) histograms, average waveform and overall variance between waveforms assigned to one unit. Sorted spikes were separated based on timestamps and assigned separately to ZT 2 and ZT 7 before further quantifications were performed. The firing rate in each vigilance state was calculated for each unit as the count of spikes per 1 s in the relevant vigilance state. Units that have firing rate below 0.1 Hz

in general or at any vigilance state have been excluded to avoid units with scarce firing. For each unit ≥ 0.1 Hz, the firing rate was expressed as relative values (firing rate ZT 7/ZT 2 in the same vigilance state).

Population ON and OFF analysis was performed using similar approach as Vyazovskiy et al. (2009).[18]Timestamps for units belonging to the same tetrode were concatenated in one matrix, and then summed to a binary vector where 0 represents no firing and ≥ 1 represents spike activity within tetrode. Onset and offset of silent periods (periods with no spikes activity within tetrode units) were detected and only silent periods that lasted ≥ 50 ms (ms) were defined as "OFF" and considered for further analysis. Similarly, activity periods were considered as segments within our binary vector that were interrupted by OFF-periods. Only segments of activity that lasted between 50 and 4000 ms and contained at least 10 spikes were defined as "ON". We detected ON and OFF periods for each vigilance state and quantified their duration and incidence. ON firing rates were calculated for each ON period as the count of spikes per ON period length and averaged across all ON-periods detected in the relevant vigilance state.

Local micro-infusion through cannula

Mice were placed in a chamber of isoflurane (1.5–2%) for anesthesia for less than 3 min then internal acute guide (Plastics One Inc., #C315IA, 0.6 mm with 0.3 mm projection) was inserted inside cannula, and 1.5 μL of relevant substance was infused with the rate of 250 nL/min. The infusion lasted ≈ 7 min and the internal acute guide was kept in place for ≈ 5 min before it was slowly removed. Mice recovered from anesthesia within ≈ 10 min. We excluded the hour during which injection and anesthesia occurred to avoid potential confounds from the effects of anesthesia on the EEG signal.

Optogenetic Stimulation

Stimulations were controlled by 4-channel LED driver (Thorlabs,Inc, #DC4104) connected via 4-channels hub (Thorlabs,Inc, #DC4100-HUB) to fiber-coupled LED light source (Thorlabs,Inc, #M470F3,470 nm) coupled to 400 μm core patch cable (Thorlabs,Inc, #FT400EMT-custom), and finally connected via a ceramic mating sleeve(Thorlabs,Inc, #ADAL1-5) to an implanted optrode ferrule on top of mouse head. The power at the end of optrode tip was measured prior to implantation and also at the end of experiment using power meter (Thorlabs,Inc, #PM100A), and light power at the optical fiber tip was between 5 and 10 mV. The stimulation protocols were conducted by programmable master-9 pulse generator (MicroProbes, Inc.). Three different stimulation paradigms were used in our study: 10 ms LED-on cycles separated by 90 ms intervals of LED-off (referred to as 10 ms, 10 Hz stimulation), 15 ms LED-on cycles separated by 35 ms intervals of LED-off (referred to as 15 ms, 20 Hz stimulation), and 1 s LED-on cycles separated by 4 s intervals of LED-off (referred to as 1 s per 5 s stimulation).

Transcriptomics

Experimental design

We performed 2 RNA-seq experiments: sleep deprivation vs. sleep and opto-TrkB vs. opto-ChR2. Both experiments were performed on WT mice that habituated to environment for at least 3 weeks prior to experiment. Sleep deprivation ($N = 4$) was performed using gentle handling and by introducing novel objects into home cages and started at light onset (ZT 0) for the duration of 3 h. In contrast, sleep group mice were undisturbed in their home cages. Mice were sacrificed 3 h after light onset and fraction of somatosensory cortex of the right hemisphere was dissected (area ≈ 1 mm) on ice-chilled RNase-free metal plate and immediately flash-frozen in liquid nitrogen. To characterize transcriptome signature upon locally induced SWA, we injected mice with *mCaMKIIa(short)-Opto-B(E281A)* AAV5 or *mCaMKIIα-hChR2(H134R)* AAV5, targeting the somatosensory cortex. Mice were housed for 3 weeks to allow sufficient time for viral expression before they were implanted with optrodes on injection site. Mice habituated to optical cables for at least 6 days prior to stimulations. Stimulation (For opto-TrkB ($N = 5$):1s per 5s and for opto-ChR2($N = 3$): 10 ms,10Hz) was performed at light onset for duration of 3 h (ZT 0-3) before mice were sacrificed. Injection/optrode site was dissected on ice-chilled RNase-free metal plate and immediately flash-frozen in liquid nitrogen.

RNA-Seq &analysis

RNA extraction was performed using total RNA purification Micro-Kit (NORGEN CORP., #35300,35350). We obtained at least 700 ng of RNA per sample with RNA Integrity Number (RIN) between 7.2 and 8.8 (Agilent Technologies Inc., Agilent RNA ScreenTape Quick, #Agilent 4200). Quality control and sequencing was done at Functional Genomics Center Zurich FGCZ (Library Protocol:Illumina Truseq mRNA; Instrument: Illumina Novaseq 6000; Read Configuration: Single Read 100 bp).Transcripts abundance were quantified using Kallisto algorithm and differential gene expression analysis was performed using DESeq2 R package via FGCZ-SUSHI interactive webtool. We detected 15194 transcripts in sleep deprivation vs. sleep condition and 15642 in optoTrkB vs. opto-ChR2 condition, and significance threshold were adjusted to $p < 0.05$ and $|\log2$ fold change$| \geq 1$. Enrichments analyses were analyzed on significant upregulated transcripts, using all detected transcripts in our dataset as a background. GESA (Figure 1D) was obtained via Enrichr bioinformatic webtool using Bioplanet_2019 database.[149,150] Transcripts-interaction network (Figure 1C) was created using STRING (v11.5) with default parameter with high confidence (0.700) as minimum required interaction score and clustering of interaction networks were achieved using the Markov Cluster Algorithm (MCL) with default parameters.[151,152] We obtained 3 clusters with ≥ 5 nodes (i.e., transcripts), and the top-cluster (highest interaction nodes, = 12 nodes) was selected and presented in Figure 1C. Reactome pathway analysis (Figures 1E, and 3D) on significantly upregulated transcripts were obtained via Enrichr-KG[139] tool using reactome_2022 database. Transcription factor enrichment analysis (Figure 3E and 3F) was performed on significantly upregulated transcripts, using all detected transcripts as background, via ShinyGO 0.77 bioinformatic webtool[140] using TF.target

TFRegNetwork database,[153] and only significantly (FDR-adjusted *p*-value <0.05) enriched terms with ≥3 genes were considered. Heatmaps were plotted using Morpheus (https://software.broadinstitute.org/morpheus/) with a range of fixed colors between minimum −1 and maximum 1).

Proteomics

Experimental design

Proteomics experiments were designed and performed similar to transcriptomics experimental design, with some modifications. To estimate the amount of protein that we could obtain from a local cortical area of approximately 1–2 mm, we conducted pilot experiments and found that we could yield ≈40 μg per mouse. As a result, we pooled together the extracted local areas from 3 mice and were further processed as one sample. Furthermore, samples were extracted directly into ice-cold homogenization buffer (2M sucrose, 0.5M HEPES, pH 7.4) supplemented with complete protease inhibitor cocktail (Roche, 0.05 mM dithiothreitol (DTT), 0.1 mM phenylmethylsulfonyl fluoride, and 20 U/10 μL RNaseOUT, Invitrogen). (Sleep group: *n* = 3 samples collected from 9 mice; Sleep dep. group: *n* = 3 samples collected from 9 mice; opto-TrkB group: *n* = 3 samples collected from 9 mice; opto-ChR2 group: *n* = 3 samples collected from 9 mice).

Sample preparation

Samples were processed as described in Noya et al. (2019)[35] and Brüning et al. (2019),[154] and lysis protocol was adapted from Humphrey et al. (2018).[155] In detail, samples were homogenized using a Teflon-glass tissue grinder using a motor-driven pestle keeping samples cooled. Homogenates were lysed in SDC lysis buffer [2% (w/v) Sodium deoxycholate, 100 mM Tris-HCl, pH 8.5] supplemented with protease and phosphatase inhibitors [0.1mM EDTA, 0.5mM DTT, 1μM PMSF, 10mM NaF, 10mM Na3VO4], boiled for 5 min at 95°C, then cooled on ice for 5 min, followed by a sonication step using a Bioruptor (high-power setting at 4°C for 15 min,15 cycles of 30 s). Volumes were adjusted with lysis buffer and samples were reduced and alkylated by adding 1:10 alkylation buffer [final 10mM TCEP HCl (Tris(2-carboxyethyl) phosphine hydrochloride), 40mM 2-chloroacetamide, pH 7]. After incubation at 45°C for 5 min at 1500rpm, the protein was digested by 1:100 (protein: enzyme) trypsin and LysC overnight at 37°C at 1500rpm. A 100 μL loading buffer [99% Isopropanol, 1% TFA] were added to 3 μg protein digest and all peptides were then loaded onto self-made non-equilibrated SDB-RPS (styrene divinylbenzene–reversed phase sulfonated) StageTips (47mm, #2241, 3M Empore), centrifuged for ≈8 min, 700xg, washed with 100μL loading buffer and 100μL wash buffer [5% ACN and 0.2% TFA]. Peptides were eluted with SDB-RPS elution buffer [80% ACN, 0.3125% NH4OH] into clean PCR tubes and concentrated in a SpeedVac at 45°C under vacuum for 35–45 min until dry. Concentrated, desalted phosphopeptides and peptides were resuspended on a sonicating water bath in a buffer containing 2% ACN and 0.1% TFA. The samples were stored at −20°C until LC-MS/MS analysis.

Mass-spec & analysis

Proteome samples were measured in a single-shot manner, loading desalted peptide samples onto a 50-cm reversed-phase column (diameter 75 mm; packed in-house with 1.9 mm C18 ReproSil particles; Dr. Maisch GmbH). The column was mounted to the EASY-nLC 1200 system (ThermoFisher Scientific) and its temperature maintained at 60°C. The peptides were eluted with a binary buffer system consisting of buffer A (0.1% formic acid) and buffer B (80% ACN and 0.1% formic acid). A gradient length of 120 min was chosen (5–30% buffer B for 105min, to 95% for 10min, constant for 5min) with a flow rate of 300 nL/min. Peptides were then electro-sprayed into an Exploris 480 mass spectrometer (MS) (ThermoFisher Scientific), obtaining full scans (350–1000 m/z, R = 120,000, max. injection time 45ms, normalized AGC target 300%). Data-independent acquisition of MS2 spectra was performed with equally sized 4.8 m/z windows with an overlap of 1 m/z (R = 15,000, automatic max. injection time, normalized AGC target 1000%, HCD Collisonal Energy 30%).

Raw MS data files were processed using DIA-NN[156] (v1.8.1) with default parameters, except for a max peptide length of 35. A spectral library was generated from FASTA files of the UniProt database from mouse with isoforms (October 2022), the output was filtered at 0.01 FDR, and the MaxLFQ algorithm, as implemented in the R library diann, was used to normalize protein quantifications. Data were then processed using the Perseus Software[138] (v1.6.10.50). MaxLFQ data were log2 transformed and one control sleep (No.04), one opto-TrkB (No.08) samples were removed due to low quantifications. Two conditional pairs were made (sleep vs. sleep deprivation, opto-ChR2 vs. opto-TrkB) and filtered for 70% valid values in at least one group in each pair. Then, missing data was imputed from a normal distribution of each sample separately with a width of 0.3 and a downshift of 1.8.

We quantified 2950 proteins in the proteome comparison between opto-TrkB vs. opto-ChR2 and 4818 proteins in comparison between sleep deprivation vs. sleep. Common samples contaminants (i.e., keratin proteins) have been filtered out of the data (5 proteins in TrkB vs. ChR2 and 14 proteins in sleep deprivation vs. sleep). Significance thresholds were adjusted to student-t-tests *p* = 0.05 and |log2 fold change| ≥ 0.5. Enrichments of GO-CC terms were analyzed on significantly upregulated proteins, using all quantified proteins in our dataset as a background, via ShinyGO 0.77 bioinformatic webtool (cutoff FDR 0.05, ≥3 proteins per pathway).[140] Protein-protein interaction networks for significantly upregulated proteins were created using STRING (v11.5) with high confidence (0.700) as minimum required interaction score, and clustering of interaction networks were achieved using the Markov Cluster Algorithm (MCL, inflation parameter = 2).[151,152] We obtained 2 significant clusters with interaction nodes ≥6. GO BP enrichment analysis on each cluster gene set was performed using all detected proteins in our dataset as a background. A heatmap of the Z score of the log2 LFQ intensity of differentially abundant proteins was plotted using Morpheus (https://software.broadinstitute.org/morpheus/) with the range of fixed colors between minimum −2 and maximum 2.

Computational model and simulation

A computational model is constructed to mimic a cortical neuron network that consists of both excitatory pyramidal and inhibitory interneurons. Each neuron is a single-compartment Hodgkin-Huxley type of model that incorporates a series of intrinsic ion channels that have been extensively studied in Hill and Tononi 2005,[157] Bazhenov et al. (2002),[158] Compte et al. (2003),[159] and Tatsuki et al. (2016)[160] (see below for more details). The network has 250 neurons, of which 90% are excitatory with NMDA and AMPA receptors, and 10% are inhibitory with GABA-A receptors. The neurons are randomly connected to 2% of the total population and are conductance coupled: when a neuron fires, it will activate the synaptic channel of the post-synaptic neuron and generate a post-synaptic current:

$$\frac{ds}{dt} = \alpha_s T_i^{in} - \frac{s}{\tau_s}$$

where s is the gating variable of either NMDA, AMPA or GABA channel of the post-synaptic neuron. T_i^{in} is the weighted input that the i th neurons receive from its pre-synaptic neurons:

$$T_i^{in} = \frac{1}{N}\sum_j w_{ij} T_j^{out}$$

Here the neuron output T^{out} is modeled as a sigmoidal function based on its voltage, w_{ij} is the weight from the j th neuron to the i th neuron, and N is the number of pre-synaptic connections that the i th neuron has. We vary the weights w_{ij} by assigning random values according to a normal distribution of different means and standard deviation. Each network is simulated for 60 s with random initial conditions. All equations are solved with the fourth-order Runge-Kutta method with computer codes written in MATLAB 2022.

As we described above, each neuron is modeled as a single-compartment Hodgkin-Huxley type of neuron, whose electrophysiology is governed by the following equation:

$$-C\frac{dV}{dt} = \left. I_L + I_{Na} + I_k + I_A + I_{KS} + I_{Ca} + I_{KCa} + I_{NaP} + I_{AR} + I_{syn} \middle/ A \right.$$

Where C and A represent the membrane capacitance and area, V is the membrane potential and I_x represents a series of ionic and synaptic currents. The choice of ionic and synaptic channels is largely based on previous sleep modeling studies [Hill and Tononi 2005,[157] Bazhenov et al. (2002),[158] Compte et al. (2003),[159] and Tatsuki et al. (2016)[160]] and contain many of the key current found in cortical neurons.

Now we describe each ionic current:

$$I_L = g_L(V - V_L)$$

$$I_{Na} = g_{Na}m^3h(V - V_{Na})$$

$$m_{Na\infty} = \alpha_m / (\alpha_m + \beta_m)$$

$$\alpha_m = 0.1(V + 33) / [1 - exp(-(V + 33) / 10)$$

$$\beta_m = 4\,exp(-(V + 53.7) / 12)$$

$$\frac{dh_{Na}}{dt} = 4(\alpha_h(1 - h_{Na} - \beta_h h_{Na}))$$

$$\alpha_h = 0.07\,exp(-(V + 50) / 10)$$

$$\beta_h = 1/[1 + exp(-(V + 20) / 10)]$$

$$I_K = g_K n_K^4(V - V_k)$$

$$\frac{dn_k}{dt} = 4(\alpha_n(1 - n_k) - \beta_n n_k)$$

$$\alpha_n = 0.01(V + 34)/[1 - exp(-(V + 34) / 10)]$$

$$\beta_n = 0.125 \, exp(-(V + 44)/25)]$$

$$I_A = g_A m_{A\infty}^3 h_A (V - V_k)$$

$$m_{A\infty} = 1/[1 + exp(-(V + 50)/20)]$$

$$\frac{dh_A}{dt} = (h_{A\infty} - h_A) \Big/ \tau_A$$

$$h_{A\infty} = 1/[1 + exp((V + 80)/6)]$$

$$I_{KS} = g_{KS} m_{KS} (V - V_k)$$

$$\frac{dm_{KS}}{dt} = (m_{KS\infty} - m_{KS}) \Big/ \tau_{KS}$$

$$m_{KS\infty} = 1/[1 + exp(-(V + 34)/6.5)]$$

$$\tau_{KS} = 8/[exp(-(V + 55)/30) + exp((V + 55)/30)]$$

$$I_{Ca} = g_{Ca} m_{Ca\infty}^2 (V - V_{Ca})$$

$$m_{Ca\infty} = 1/[1 + exp(-(V + 20)/9)]$$

$$I_{KCa} = g_{KCa} m_{KCa\infty} (V - V_K)$$

$$m_{KCa\infty} = 1 \Big/ \left[1 + \left(K_D / [Ca^{2+}] \right)^{3.5} \right]$$

$$I_{NaP} = g_{NaP} m_{NaP\infty}^3 (V - V_{Na})$$

$$m_{NaP\infty} = 1/[1 + exp(-(V + 55.7)/7.7)]$$

$$I_{AR} = g_{AR} h_{AR\infty} (V - V_K)$$

$$h_{AR\infty} = 1/[1 + exp((V + 75)/4)]$$

The synaptic current consists of three components since each neuron can receive NMDA or AMPA signaling from excitatory neurons and GABA-A signaling from inhibitory neurons. Each synaptic current is calculated as

$$I_x = g_x s_x (V - V_x)$$

where x indicates which synaptic channel is considered, g_x is the membrane conductance of that channel, s_x is the gating variable and V_x is the reversal potential. The gating variable s_x of AMPA or GABA receptors is governed by the following equation:

$$\frac{ds_x}{dt} = a_x T^{in} - \frac{s_x}{\tau_x}$$

The gating variables of NMDA receptor is modeled as:

$$\frac{ds_{NMDA}}{dt} = 0.5 x_{NMDA}(1 - s_{NMDA}) - \frac{s_{NMDA}}{\tau_{sNMDA}}$$

And x_{NMDA} follows the equation:

$$\frac{dx_{NMDA}}{dt} = a_{NMDA}T_{in} - \frac{x_{NMDA}}{\tau_{xNMDA}}$$

Each neuron's synaptic input T_{in} is calculated as a weighted average of all the synaptic output from its pre-synaptic neurons:

$$T_i^{in} = \frac{1}{N}\sum_j w_{ij}T_j^{out}$$

where each neuron's output T^{out} is modeled as a sigmoidal function:

$$T_{out} = \frac{1}{1 + exp(-(V - V_T)/K_T)}$$

When a pre-synaptic neuron fires, it will generate a synaptic input that excites the post-synaptic neuron's synaptic channel and further generates a synaptic current. All parameters used in the simulation are presented in Table S2 and aligned with values investigated in Tatsuki et al. (2016).[160] The electrophysiology equations are solved with fourth-order Runge-Kutta method with computer codes written in MATLAB 2022.

Modifying synaptic strength

In our network, we simulate 250 neurons where 225 are excitatory and 25 are inhibitory. Each neuron is randomly connected to 2% of the other neurons, whether inhibitory or excitatory. Then we randomly assign weights to the 1250 connections following a normal distribution with certain mean $\overline{w}$ and relative standard deviation σ that we vary as indicated. We simulate the network with 20 different levels of $\overline{w}$ and 10 levels of σ. With increasing magnitude of $\overline{w}$, we try to model the potentiation induced by BDNF, and we model the realistic distribution of synaptic weights with different levels of σ.

GABA knock-out

When we try to model the knock-out of GABA-A signaling in the network, we put g_{GABA} of all neurons to be 0 such that neurons will not receive any inhibitory current. All the other simulation parameters are as before.

Current Injection

To model the firing rate increase, an applied current of 1 μA was applied to all neurons in the network for 10 s in the simulation presented in Figure 5H from t = 20s to t = 30s.

Data Collection

Local field potential data is calculated by averaging the voltage of the whole 250 neurons, sampled with a frequency of 2000Hz. The LFP data is then binned into 1 s segments to calculate the spectrogram. The spectrum of the whole recording was calculated by the "pspectrum" function from MATLAB 2022.

Plotting

Bar plots represent the mean ± standard error of mean (SEM). Shaded area in the SWA time course plots represent mean ± SEM. Plots were prepared in MATLAB R2020b ("boundedline", "bar", "boxchart", "scatter"), R, and GraphPad Prism 9. Figures were prepared in free open source Inkscape software.

QUANTIFICATION AND STATISTICAL ANALYSIS

Data were tested for normality using Shapiro-Wilk test (MATLAB: "swtest") and tested for equal distribution of variance using (MATLAB: "vartest2" for 2 groups, and "vartestn" for >2 groups). Based on study design, normality, and variance; the appropriate parametric or non-parametric tests were performed with appropriate correction (i.e., Welch's correction), when needed. Effect size was calculated using Cohen's test (MATLAB: "computeCohen_d") and reported for significant comparison as d in the legends. For SWA time-course comparison between hemispheres, we performed 2-way repeated measures ANOVA (2-way RM ANOVA) on the interaction between (hemisphere x time bins) on the hours that are marked by the horizontal line (see figures) following manipulations. In case of missing data points (i.e., a mouse that did not have enough artifact-free NREM epochs "less than 150 s within an hour", we performed mixed-effects model "REML" instead, and the p-value of the interhemispheric comparison was reported in the legends. For power spectrum interhemispheric comparisons, we performed paired student t-tests. All tests were performed in MATLAB R2020b ("signrank", "ranksum", "ttest", "ttest2", "kruskalwallis", "anova1", "friedman") except for 2-way repeated measures ANOVA and REML that were performed in GraphPadPrism9. Statistical significance was defined as $*p < 0.05$, $**p < 0.01$, $***p < 0.001$.